

AperTO - Archivio Istituzionale Open Access dell'Università di Torino

## Lithospheric magma dynamics beneath the El Hierro Volcano, Canary Islands: insights from fluid inclusions

### This is the author's manuscript

*Original Citation:*

*Availability:*

This version is available <http://hdl.handle.net/2318/1661712> since 2018-03-08T16:02:36Z

*Published version:*

DOI:10.1007/s00445-017-1152-6

*Terms of use:*

Open Access

Anyone can freely access the full text of works made available as "Open Access". Works made available under a Creative Commons license can be used according to the terms and conditions of said license. Use of all other works requires consent of the right holder (author or publisher) if not exempted from copyright protection by the applicable law.

(Article begins on next page)

**This is the author's final version of the contribution published as:**

OGLIALORO E., FREZZOTTI M.L., FERRANDO S., TIRABOSCHI C., PRINCIPE C., GROPPPELLI G., VILLA I.M.: Lithospheric magma dynamics beneath the El Hierro Volcano, Canary Islands: insights from fluid inclusions. Bull. Volcanol., 79 (2017), 70, doi: 10.1007/s00445-017-1152-6.

**The publisher's version is available at:**

<http://link.springer.de/link/service/journals/00445/index.htm>

**When citing, please refer to the published version.**

**Link to this full text:**

<http://hdl.handle.net/2318/332747>

This full text was downloaded from iris-AperTO: <https://iris.unito.it/>

[Click here to view linked References](#)

# Lithospheric magma dynamics beneath El Hierro volcano, Canary Islands: insight from fluid inclusions

*E. Ogialoro<sup>1</sup>, M.L. Frezzotti<sup>1</sup>, S. Ferrando<sup>2</sup>, C. Tiraboschi<sup>1</sup>, C. Principe<sup>3</sup>, G. Groppelli<sup>4</sup>, I.M. Villa,<sup>1,5,6</sup>*

*1-Dipartimento di Scienze dell'Ambiente e della Terra, Università di Milano Bicocca, 20126 Milan, Italy*

*2-Dipartimento di Scienze della Terra, Università di Torino, 70125 Turin, Italy*

*3-Istituto di Geoscienze e Georisorse, Consiglio Nazionale delle Ricerche, 56121 Pisa, Italy*

*4-Istituto per la Dinamica dei Processi Ambientali-sezione di Milano, Consiglio Nazionale delle Ricerche, 20131 Milan, Italy*

*5-Institut für Geologie, Universität Bern, 3012 Bern, Switzerland*

*6-Centro Universitario Datazioni e Archeometria, Università di Milano Bicocca, 20126 Milano, Italy*

*Corresponding author: Maria Luce Frezzotti maria.frezzotti@unimib.it*

**Keywords** El Hierro, petrology, fluid inclusions, mantle xenoliths, magma transport

## Abstract

In active volcanoes, petrological studies have been proven to represent a reliable approach to defining the depth conditions of magma transport and storage in the mantle and the crust. Based on fluid inclusion mineral geothermobarometry in mantle xenoliths, we propose a model for the recent magma plumbing system of the Island of El Hierro (Canary Islands). Studied peridotites are entrained in a lava flow from El Yulan Valley, which is part of the Rift volcanism activity at approximately 40-30 ka. Peridotites are spinel lherzolites, harzburgites and dunites equilibrated in the shallow mantle at pressures from 1.5 to 2 GPa. 800 to 950°C (LT peridotites).

31 and higher equilibration temperatures from 900 to 1100°C (HT peridotites). Microthermometry  
32 and Raman analyses of fluid inclusions show trapping of two distinct fluid phases: early Type I  
33 metasomatic CO<sub>2</sub>-N<sub>2</sub> fluids ( $d = 1.19 \text{ g/cm}^3$ ), coexisting with silicate-carbonate melts, in LT  
34 peridotites; and late Type II pure CO<sub>2</sub> fluids ( $d = 0.99$  to  $1.11$  and  $0.65 - 0.75 \text{ g/cm}^3$ ) in both LT  
35 and HT peridotites. Type I fluids represent metasomatic phases in the deep oceanic lithosphere  
36 (60-65 km) before the onset of magmatic activity, whereas Type II CO<sub>2</sub> fluids testify for fluid  
37 trapping episodes during the ascent of xenoliths in host mafic magmas. Identification of magma  
38 accumulation zones through interpretation of Type II CO<sub>2</sub> fluid inclusions and mineral  
39 geothermobarometry indicate the presence of a vertically stacked system of interconnected small  
40 magma reservoirs in the shallow lithospheric mantle from 22 to 36 km depth (or 0.67 to 1 GPa).  
41 This deeper magma accumulation region fed a short-lived magma storage region located in the  
42 lower oceanic crust at 10 - 12 km depth (or 0.26–0.34 GPa). According to our model, the 40-30  
43 ka old volcanic activity of El Hierro is related to mantle magma dynamics, as also proposed for  
44 the 2011-2012 eruption.

45

## 46    **Introduction**

47

48            A central question for forecasting eruptive behavior in active volcanoes is the  
49    architecture of the magma plumbing system, which exerts a critical control on the  
50    compositional variation of magmas, the depths and conditions at which they are stored, and  
51    their residence time at different crustal/mantle levels (e.g., Sparks 2003; Peccerillo et al. 2006;  
52    Scandone et al. 2007).

53            Multiple and complementary studies combining both geophysical and petrological  
54    approaches are applied to get insights into the internal structure of volcanoes (e.g. Bertagnini  
55    et al. 2003; Schwarz et al. 2004; Morgan et al. 2007; Stroncik et al. 2009). Among petrological  
56    studies, fluid inclusion and mineral geothermobarometry provide information on the depths of  
57    magma ponding and crystallization (c.f. Andersen and Neumann 2001; Frezzotti and  
58    Peccerillo 2004; Hansteen and Klügel 2008). Fluid inclusions, in fact, record pressures of  
59    trapping at and changes of fluid density in response to magma pressure variations on short  
60    time scales (Peccerillo et al. 2006). They are therefore sensitive probes of discrete magma  
61    storage regions.

62            This approach has been successfully applied to several active volcanoes both in the  
63    oceanic and continental lithosphere (e.g., Hawaii, Canary Islands, Azores, and the Aeolian  
64    Islands; Roedder 1983; De Vivo et al. 1988, Frezzotti et al. 1991; Hansteen et al. 1998; Zanon  
65    et al. 2003; Zanon and Frezzotti 2013). In the Canary Islands, previous fluid inclusion studies  
66    suggested that the volcanoes are supplied by a plumbing system that delivers magma directly  
67    in the lower crust (e.g., Hansteen et al. 1991, 1998; Frezzotti et al. 1994; Andersen et al. 1995;  
68    Neumann et al. 1995; Viti and Frezzotti 2000; Klügel et al. 2005, 2015). Although fluid  
69    inclusion investigations have failed to identify magma storage regions below the Moho,

70 mineral-melt geothermobarometry indicates variable clinopyroxene crystallization from 15 to  
71 45 km depth beneath La Palma and El Hierro (Stroncik et al. 2009; Barker et al. 2015; Klügel  
72 et al. 2015).

73 At El Hierro, multidisciplinary research, undertaken since the last submarine eruption  
74 of 2011-2012, has allowed identifying the presence of two discrete magma storage regions,  
75 located in the lower oceanic crust and the lithospheric mantle, respectively (Meletlidis et al.  
76 2012; Becerill et al. 2013b; González et al. 2013; Martí et al. 2013a, b; Longpré et al. 2014;  
77 Klügel et al. 2015; Carracedo et al. 2015; Zaczek et al. 2015). As summarized by Klügel et al.  
78 (2015), eruptive magma transport in the oceanic crust is characterized by sub-horizontal and  
79 lateral pathways forming temporary deep sheet intrusions (sills). These are fed by a deeper  
80 reservoir in the shallow lithospheric mantle. However, the state of this sub-Moho magma  
81 storage region is not fully resolved (e.g., Martí et al. 2013a).

82 In this work, we concentrate on the reconstruction of the magma plumbing system of  
83 El Hierro volcano, focusing on magma storage in the oceanic lithospheric mantle. Following  
84 the approach of Frezzotti and Peccerillo (2004), we have performed geothermobarometry of  
85 fluid inclusions and minerals in ultramafic xenoliths from a lava flow of El Julan cliff,  
86 representative of the Rift Volcanism activity at approximately 40-30 ka (Guillou et al. 1996;  
87 Carracedo et al. 2001; Becerill et al. 2013a). Results allow modeling the internal structure of  
88 El Hierro volcano.

89

## 90 **Geological setting**

91

92 The Canary archipelago (Spain) consists of seven main volcanic islands located on the  
93 continental rise off Cape Juby (northwest Africa). It extends for roughly 500 km in a ridge

94 developed on the margin of the African Plate (Fig. 1a) (Robertson and Stillman 1979;  
95 Marinoni and Pasquarè 1994; Carracedo et al. 1999; Marinoni and Gudmundsson 2000).

96 The sub-aerial volcanic activity shows a general westwards decrease in age from 21-20  
97 Ma at Fuerteventura-Lanzarote to less than 2 Ma at El Hierro and La Palma (Fig.1a), that are  
98 at present in their shield building phase (Schmincke 1982; Guillou et al. 1996; Carracedo  
99 1999;). The islands lay on oceanic lithosphere formed during the opening of the Central  
100 Atlantic Ocean (~150-180 Ma; Hoernle 1998). The oceanic crust shows an eastward  
101 progressive thickening, from about 12 - 15 km at El Hierro to 35 km at Lanzarote (Martinez-  
102 Arevalo et al. 2013). The main regional tectonic structures have been classified in Atlantic or  
103 "oceanic" (N160–N180°E, N120–N135°E), and African or "continental" (N20°E, N45°E,  
104 N75°E) (Anguita and Hernan 1975, 2000; Fuster 1975; Geyer and Martí 2010).

105 Magmatic activity is dominated by alkali-basalts (picrites, basanites), with minor  
106 tholeiites and differentiated lavas (e.g. trachytes and phonolites). The origin of intraplate  
107 volcanic activity is still controversial (cf. Lustrino and Wilson 2007). The most popular  
108 genetic hypothesis is the mantle plume model (e.g. Hoernle and Schminke 1993; Carracedo et  
109 al. 1998; Duggen et al. 2009), although other interpretations have been proposed, including a  
110 local extensional model (Fuster 1975) and an uplifted tectonic block model (Araña and Ortiz  
111 1991). Moreover, Anguita and Hernán (2000) postulated a single unified model taking into  
112 account mantle plume dynamics combined with the regional tectonics to explain the initiation  
113 of mantle melting processes.

114 At El Hierro, the sub-aerial volcanic activity started at 1.12 Ma, with massive lava  
115 flows in the NE of the island (Guillou et al. 1996). Three main volcanic cycles are identified,  
116 namely Tiñor Edifice (1.12-0.88 Ma), Golfo-Las Playas Edifice (0.545-0.176 Ma), and Rift  
117 Volcanism (0.158 Ma - Present) (Carracedo et al. 2001; IGME 2010a, b, c, d; Becerril et al.

2013a). These cycles are separated by quiescence, structural deformation and sector collapses. Sector collapses formed four main amphitheaters: Las Playas I and II (~545-0.176 and 0.176-0.145 Ma, respectively), El Julan (~ 0.158 Ma) and the Golfo (~ 87-39 ka) (Masson 1996; Masson et al. 2002; 2006; Gee et al. 2001; Longpré et al. 2011). Erupted lavas increase in alkalinity and degree of evolution through time (Stroncik et al. 2009). Lavas of Tiñor volcano are picritic to hawaiitic-tephritic in composition, whereas those of the Golfo-Las Playas edifice range from basanites to trachytes and nephelinites.

The last cycle of Rift Volcanism (158 ka - Present) is characterized by cinder cones and relatively thin lava flows covering most of the island. Lavas are mainly alkali-picrites and basanites with minor tephrites (Carracedo et al. 2001). Radiometric ages ranging from 158 to 2.5 ka broadly constrain the Rift Volcanism activity (Guillou et al. 1996; Carracedo et al. 2001). Over the last 600 years, a single submarine monogenic eruption occurred in La Restinga area in 2011-2012 (e.g. Lopez et al. 2012; Martí et al. 2013a, b; Longpré et al. 2014).

Abundant ultramafic xenoliths are reported in several lava flows and pyroclastic rocks on the Island (Neumann 1990, Hansteen et al. 1991; Neumann et al. 2004). For the present study, xenolith samples have been collected in a locality in the El Julan Cliff Valley (27°41'27"N - 18°02'49"W), not sampled before (Fig. 1b). The outcrop consists of a massive basaltic lava flow of about 3 m thickness (Fig. 2a), which is part of a continuous succession without any significant unconformity. No dating is available for this xenolith-bearing lava flow, but its position is compatible with the Rift Volcanism activity at approximately 40-30 ka. In fact, Carracedo et al. (2001) dated two lava flows in this area (~ 1 km southwest) at 41 and 31 ka, respectively (K-Ar dating).

140

141



## 142    **Analytical techniques**

143

144        Peridotite modal compositions have been defined by multicolor image analysis  
145 (ImageJ and Photoshop C5 softwares), reconstructing the total pixel areas of minerals  
146 identified in thin sections.

147        A Wavelength Dispersive System (WDS) microprobe has been used for major element  
148 composition of mineral phases, using double-polished thick sections. WDS analyses have been  
149 performed with a JEOL JXA 8200 Superprobe, equipped with five wavelength-dispersive  
150 spectrometers, Energy Dispersive X-ray spectroscopy (EDS), and cathodoluminescence  
151 detectors at the University of Milano. The operating conditions consist of an acceleration  
152 voltage of 15 kV, at a beam current of 15 nA at 30s counting time, with a spot size of 1  $\mu\text{m}$ .  
153 The typical detection limit for each element was 0.01%. Natural and synthetic minerals have  
154 been used as standards, within 2% at  $2\sigma$  standard deviation. Structural formulae of minerals  
155 have been processed through the software NORM of Ulmer (1986).

156        Fluid inclusion microthermometry has been carried out with a Linkam THMS600  
157 heating/freezing stage, equipped with a Leitz microscope (40 $\times$  objective), which operates in a  
158 temperature range between -196 and 600°C at the University of Milano Bicocca. The  
159 instrument was calibrated checking CO<sub>2</sub> and H<sub>2</sub>O triple points (-56.6°C and 0.1°C,  
160 respectively) in natural and synthetic fluid inclusions (SYN-FLINC). In the temperature  
161 interval from -90 to 31°C, an accuracy of  $\pm 0.1$  °C has been estimated at the standard reference  
162 points, and of  $\pm 0.2$  °C at the other temperatures. The melting temperature ( $T_m$ ) and the  
163 homogenization temperature ( $T_h$ ) of fluid inclusions have been measured with a heating rate  
164 variable from 0.3 to 0.1 °C/min. The density of CO<sub>2</sub> inclusions has been calculated by the  
165 equation of Duschek et al. (1990) (BULK software; Bakker 2003). Isochores have been

166 determined using the equation of Holloway (1981) (ISOCHORE software; Bakker 2003). The  
167 selected equation is valid up to least 2000 °K and 1.5 GPa. Molar volumes of CO<sub>2</sub>-N<sub>2</sub> fluids  
168 have been derived by plotting fluid composition determined by Raman spectroscopy and  
169 temperature of measured sequences of phase transitions in the isochoric (cm<sup>3</sup>/mole) CO<sub>2</sub>-N<sub>2</sub> T-  
170 X diagram of van den Kerkhof (1988) and Klemm et al. (1992). Isochores for CO<sub>2</sub>-N<sub>2</sub> fluid  
171 inclusions have been calculated using the equation of Holloway (1977) valid from 373 to 1273  
172 °K and up to 2 GPa, (ISOCHORE software; Bakker 2003).

173 Fluid inclusions have been further analyzed by Raman microspectroscopy (Horiba  
174 Labram HR800) at the "G. Scansetti" Center of the University of Torino. A polarized Nd  
175 green laser operating at 532 nm wavelength and 80 mW emission power was used as the  
176 excitation source, with a spot size resolution of 1x1x3 µm. The slit width was 300 µm, the  
177 grating was 600 grooves/mm, and the corresponding spectral resolution was  $\pm 1.5 \text{ cm}^{-1}$ .  
178 Raman spectra have been collected with a 100× Olympus objective and 3 accumulations of  
179 30s. The calibration of the instrument has been daily checked by the 521 cm<sup>-1</sup> silicon band.  
180 The determination of the relative molar fractions of end-member components in CO<sub>2</sub>-N<sub>2</sub>  
181 mixtures, as well as the characterization of daughter minerals in fluid inclusions, have been  
182 made following Frezzotti et al. (2012; and references therein). Spectra statistical fitting has  
183 been performed with Fityk 0.9.8 free analysis software, applying PseudoVoigt functions.

184 The "Raman densimeter" (e.g. Rosso and Bodnar 1995) for pure CO<sub>2</sub> fluid inclusions,  
185 based on the distance of the CO<sub>2</sub> Fermi doublet ( $\Delta$ , in cm<sup>-1</sup>; Wang and Wright 1973; Garrabos  
186 et al. 1980) has been applied using the equation of Kawakami et al. (2003) with an accuracy  
187 better than 5% in the density range from 0.1 to 1.24 g/cm<sup>3</sup>. Selection of the Raman densimeter  
188 equation was performed comparing CO<sub>2</sub> density values derived from microthermometry with  
189 those calculated by Raman analyses applying existing equations (cf., Frezzotti et al. 2012) in

190 20 fluid inclusions. The equation of Kawakami et al. (2003) resulted as the most accurate for  
191 studied fluid inclusions.

192

## 193 **Composition and P-T equilibration conditions of peridotites**

194

195 Ultramafic xenoliths are angular in shape and about 8-10 cm in size on average (Fig.  
196 2a). They have a pale green color, characteristic for fresh peridotites. The rock contours are  
197 sharp and lava infiltrations are generally absent. The host basanitic lava is unaltered,  
198 porphyritic, and consists of olivine and Ti-augite phenocrysts (30 vol%) in a glassy  
199 groundmass. Among collected samples, 11 peridotites have been selected for petrological and  
200 fluid inclusion studies.

201

## 202 Petrography and mineral chemistry of peridotites

203 Studied rocks are type I peridotites (Frey and Prinz 1978) and consist of 3 spinel  
204 dunites (Ol 92-94, Cpx 1-4, Opx 4-6 vol%; samples XML 1, 5, and 10), 3 spinel lherzolites  
205 (Ol 63-78, Cpx 11-12, Opx 11-26 vol%; samples XML 3, 6, and 8) and 5 spinel harzburgites  
206 (Ol 59-78, Cpx 2-4, Opx 18-38 vol%; samples XML 4, 7, 9, 11, and 12). Most harzburgites  
207 and lherzolites have protogranular textures, with recrystallization degrees variable from 10 to  
208 30 vol%, and only one lherzolite (XML 3) grades into the porphyroclastic type. Reaction rims  
209 between xenolith and host basanite are not observed. Some peridotites contain intragranular or  
210 intergranular glass microveins which do not reach the contact with the host lava.

211 Olivine and orthopyroxene are present as strained porphyroclasts (4 - 25 mm in size)  
212 and smaller polygonal strain-free neoblasts ( $\leq 2$  mm in size). Olivine porphyroclasts (Ol I) are

213 typically coarse-grained, with several grains up to 25 mm in size. Olivine porphyroclasts show  
214 kink-bands (Fig. 2b) and may contain trails of spinel inclusions. Orthopyroxene  
215 porphyroclasts (Opx I) have similar sizes. In less recrystallized protogranular harzburgites and  
216 lherzolites (about 10-20 vol% neoblasts), they show clinopyroxene  $\pm$  spinel exsolution  
217 lamellae (Fig. 2c). In more recrystallized protogranular peridotites and in the porphyroclastic  
218 lherzolite, Opx I shows clear rims (Fig. 2d) or does not contain exsolution lamellae (Fig. 2e).

219 Olivine and orthopyroxene neoblasts (Ol II and Opx II) occur as interstitial grains or as  
220 aggregates of polygonal grains showing triple junctions. They are strain-free and can include  
221 minute spinel grains (Fig. 2f). In spinel dunites, Ol II grains are present distributed along  
222 preferred orientations, showing a rock foliation cutting large Ol I (Fig. 2h). Clinopyroxene and  
223 spinel have smaller sizes on average (1 mm) than Ol I and Opx I and occur both as subhedral  
224 and as interstitial grains. They may form symplectites with orthopyroxene and olivine (Fig.  
225 2g).

226 In spinel harzburgites and lherzolites, olivine has a narrow Mg# ( $\text{Mg\#} =$   
227  $(\text{Mg}/\text{Mg} + \text{Fe}_{\text{tot}})$ ) ranging from 0.89 to 0.91, with slightly higher values in harzburgites. CaO  
228 content varies from 0.01 to 0.17 wt% and NiO from 0.31 to 0.48 wt%. No significant chemical  
229 variation between porphyroclasts and neoblasts has been observed, except for a higher CaO  
230 content, up to 0.17 wt%, in neoblasts. Opx I and Opx II also show similar and narrow Mg#  
231 interval, from 0.90 to 0.91.  $\text{Al}_2\text{O}_3$  contents range from 2.1 to 3.7 wt%,  $\text{Cr}_2\text{O}_3$  from 0.24 to 0.7  
232 wt% and CaO from 0.36 to 0.81.  $\text{TiO}_2$  content is very low ( $< 0.17$  wt%). Clinopyroxene is Cr-  
233 diopside with Mg# ranging from 0.89 to 0.93.  $\text{Cr}_2\text{O}_3$  varies from 0.48 to 1.1 wt%,  $\text{Al}_2\text{O}_3$   
234 ranges from 1.68 to 4.55 wt% and  $\text{TiO}_2$  from 0 to 1.25 wt%. Spinel is a magnetite-spinel solid  
235 solution with a Cr# [ $\text{Cr\#} = \text{Cr}/(\text{Cr} + \text{Al})$ ] variable from 0.25 to 0.35.  $\text{Cr}_2\text{O}_3$  content ranges  
236 from 20.84 to 28.98 wt% and  $\text{TiO}_2$  from 0 to 0.22 wt%. Chromite-rich rims ( $\text{Cr\#} = 0.4 - 0.5$ )  
237 are observed in some grains.

238

239 Mineral geothermobarometry

240         Equilibration temperatures for peridotites were estimated considering the partitioning  
241 of  $\text{Fe}^{2+}$ , Mg and Ca between orthopyroxene and clinopyroxene (Wells 1977; We), the two-  
242 pyroxene and the Ca-in-opx thermometers (Brey and Koehler 1990; BK2px and BKopx), and  
243 the solubility of Ca and Al in orthopyroxene in equilibrium with olivine, clinopyroxene and  
244 spinel (Witt-Eickschen and Seck 1991; WS). Temperature estimates were performed in  
245 exsolved porphyroclasts cores and clear porphyroclasts and neoblasts of harzburgites and  
246 lherzolites.

247         Exsolved Opx I porphyroclasts provide equilibration temperatures comprised between  
248 800 and 950°C. BK2px thermometer provides the lowest equilibration temperatures at 800°C,  
249 while the We and BKopx thermometers give consistent temperatures, ranging from 800 to  
250 920°C. WS thermometer provides the highest estimates, with temperatures reaching 950°C.

251         Clear Opx I thermometry yields higher temperatures, compared to the exsolved  
252 porphyroclast thermometry, ranging from 900 to 1100°C. BK2px thermometer provides also  
253 in this case the lower estimates with temperatures of approximately 900°C. We and BK opx  
254 thermometers yield to more elevated T conditions, reaching 980°C. WS thermometer gives the  
255 higher equilibration temperatures, from 950 to 1100°C. Temperatures estimates in neoblasts  
256 show that peridotites from El Hierro have been locally heated to  $T > 1100^\circ\text{C}$  (We and BK  
257 thermometers).

258         From petrography and mineral geothermometry, it is possible to distinguish two groups  
259 of peridotites: a first group is represented by harzburgites and lherzolites that present exsolved  
260 Opx I porphyroclasts, which show equilibration temperature from 800 to 950°C (LT  
261 peridotites; XML 7, 8, 10 and 11). A latter group corresponds to harzburgites and lherzolites

262 that contain clear Opx I porphyroclasts and higher equilibration temperatures from 900 to  
263 1100°C (HT peridotites; XML 3, 4, 5 and 9). In peridotites from El Hierro and the other  
264 Canary Islands, a bimodal temperature distribution, in the same temperature intervals, was  
265 previously reported by Neumann et al. (2002; i.e., HEXO and HTR peridotites).

266 Pressures were estimated employing the Koehler and Brey (1990; KB) geobarometer,  
267 which considers the diffusion of calcium in olivine. The minimum equilibration pressures  
268 correspond to 1.5 GPa, while the maximum conditions reach pressures of 2 GPa. It has to be  
269 noted, however, that the KB barometer is strongly temperature dependent; consequently,  
270 pressure estimates have to be considered affected by a significant uncertainty.

271

## 272 **Fluid inclusion study**

273

### 274 Petrography of fluid inclusions

275 Nine representative samples of LT and HT peridotites were selected for fluid inclusion  
276 analysis. They consist of 3 dunites (XML 1, 5, and 10), 4 harzburgites (XML 4, 7, 9 and 11),  
277 and 2 lherzolites (XML3 and 9). Fluid inclusions are present in Ol I, Opx I and in  
278 clinopyroxene and are more abundant in LT peridotites. Neoblasts of Ol II and Opx II do not  
279 contain fluid inclusions.

280 Two main fluid inclusion assemblages (Roedder 1984; Bodnar 2003) have been  
281 recognized. Early Type I fluid inclusions are present only in Ol I and exsolved Opx I of LT  
282 peridotites (Fig. 3). Inclusions have rounded or negative-crystal shapes and sizes from  $\leq 3 \mu\text{m}$   
283 to  $50 \mu\text{m}$  in length. They occur either in spatially isolated small clusters or as short

284 intragranular trails often along preferred crystallographic orientations (Fig. 3a-c). Type I  
285 inclusions are often associated with carbonate-rich inclusions and glass veins (Fig. 3b).

286 At room temperature, inclusions are CO<sub>2</sub>-rich and single-phase (L; Fig. 3c), or they can  
287 contain several daughter minerals (i.e., carbonates, or carbonates + sulfates ± chlorides ±  
288 phosphates) and an opaque mineral (two-phase L+S inclusions; Fig., 3a, and d). The  
289 composition of daughter mineral phases has been determined by Raman microspectroscopy  
290 mapping (Fig. 4a). Carbonates are dolomite, or Mg-calcite and magnesite; sulfates include  
291 anhydrite, sulfohalite, and MgSO<sub>4</sub>\*nH<sub>2</sub>O; phosphate is apatite; the opaque phase is either  
292 spinel, or magnetite, or hematite (Fig. 4 b-f).

293 The second fluid inclusion assemblage is represented by late Type II CO<sub>2</sub> fluid  
294 inclusions. Type II inclusions were trapped at later stages in Ol I, Opx I and clinopyroxene of  
295 both LT and HT peridotites. They occur as intragranular and intergranular trails of variable  
296 length and as isolated clusters (Fig. 5a, c). In exsolved Opx I, Type II inclusions are observed  
297 along preferential crystallographic orientations (e.g., 010; Fig. 5d). Inclusions have negative-  
298 crystal or rounded shapes and sizes ranging from less than 1 to 40 μm in length (Fig. 5b). At  
299 room temperature, they are single phase CO<sub>2</sub> (L) or, less commonly, two phase inclusions  
300 (L+V; Fig. 5) and do not contain daughter minerals. Decrepitation textures are frequently  
301 observed, particularly in HT peridotites (Fig. 5b and d).

302

### 303 Composition and density of fluid phases

304 The chemical composition and the density of Type I and II fluid inclusions have been  
305 determined by microthermometric and Raman microspectroscopic analyses. For those Type II  
306 inclusions with a size < 3μm, density has been calculated by the “Raman densimeter”  
307 (Kawakami et al. 2003).

308

309 *Type I fluid inclusions.*

310 Phase transitions have been observed in 15 single-phase (L) Type I inclusions of two  
311 LT peridotites in the temperature range from -190 to 20°C. On cooling, 14 inclusions freeze at  
312 temperatures variable from -95 to -80°C. On subsequent heating, inclusions show slow  
313 melting of solid CO<sub>2</sub> in a 2-3°C interval, with initial melting (Ti) recorded at about -60°C, and  
314 final melting (Tm) from -58.6 to  $-56.9 \pm 0.1$  °C (Fig. 6). Homogenization temperatures to the  
315 liquid phase (ThL) range from -52.0 to  $8.0 \pm 0.1$  °C. According to the classification of van den  
316 Kerkhof (1988), the recorded phase transitions (Ti; S+L→S+L+V, Tm; S+L+V→ L+V, ThL;  
317 SL+V→L) classify H3 type CO<sub>2</sub>-rich inclusions containing minor additional gaseous species.

318 A single Type I inclusion (~ 10 µm in size, red arrow in Fig. 7a) shows a different  
319 microthermometric behavior. On cooling down to -190°C, solid CO<sub>2</sub> nucleation occurs in  
320 presence of a liquid and a vapor phase (L+S+V). On heating, four subsequent phase transitions  
321 are recorded. Partial homogenization in the presence of solid CO<sub>2</sub> (ThS; S+L+V→S+L) occurs  
322 at about -152°C; then, a small bubble re-appears at -95°C (Ti; S+L→S+L+V). On further  
323 heating, the partial homogenization in the presence of solid CO<sub>2</sub> (ThS; S+L+V→S+L) is  
324 measured at  $-61.0 \pm 0.1$  °C. The last phase transition takes place by dissolution of solid CO<sub>2</sub> in  
325 a one-phase liquid-like fluid (Ts; S+L→L) at  $-60.0 \pm 0.1$  °C. According to van den Kerkhof  
326 (1988), the observed sequence of phase transitions (S4 type fluid inclusions) identifies  
327 extremely dense CO<sub>2</sub>-N<sub>2</sub> mixtures.

328 In all analyzed Type I inclusions, the presence of nitrogen has been confirmed by the  
329 N<sub>2</sub> band from 2228 to 2330 cm<sup>-1</sup> in Raman spectra (Fig.7b and c). An N<sub>2</sub> molar fraction (X<sub>N2</sub>)  
330 of 0.18 has been calculated for the S4-type CO<sub>2</sub>-N<sub>2</sub> inclusion by quantitative Raman analysis  
331 (red arrow in Fig. 7a). H3-type inclusions contain less N<sub>2</sub>, being X<sub>N2</sub> comprised between 0.05



and 0.09 (Fig. 7a). The molar volume of CO<sub>2</sub>-N<sub>2</sub> mixtures has been derived by plotting the measured sequence of phase transitions in the CO<sub>2</sub>-N<sub>2</sub> T-X isochoric (cm<sup>3</sup>/mole) diagram (Fig. 8) of van den Kerkhof (1988) and Klemm et al. (1992). For the S4-type inclusion (X<sub>N2</sub> = 0.18 and Ths = -152°C) the corresponding molar volume is 34.5 cm<sup>3</sup>/mol (i.e. d = 1.19 g/cm<sup>3</sup>). For H3-type inclusions, molar volumes range from 38.5 cm<sup>3</sup>/mole (X<sub>N2</sub> = 0.05 - 0.09 and ThL from -52 to -51°C) to 40 - 50 cm<sup>3</sup>/mole (X<sub>N2</sub> = 0.01 and ThL from -35 to 8°C) (Fig. 7a and 8).

#### *Type II fluid inclusions.*

On cooling, Type II CO<sub>2</sub> fluid inclusions freeze at temperatures variable from -95 to -65°C. Solid CO<sub>2</sub> melts instantaneously from -57.3 to -56.5 ± 0.1°C (T<sub>m</sub>; n=50), with most measurements at -56.6 °C (Fig. 6). Melting behavior indicates that fluid inclusions consist of pure CO<sub>2</sub>, as confirmed by Raman analysis. Liquid water and/or clathrates have not been observed in any of the measured inclusions by both analytical techniques.

Type II pure CO<sub>2</sub> inclusion homogenization occurs to the liquid phase (ThL; n = 512) with a scattered distribution from -37.5 to 31.0 ± 0.1°C (Fig. 9). Only the 2% of analyzed inclusions has homogenization to the vapor phase (not shown). Interestingly, when ThL values are plotted separately for inclusions in LT and HT peridotites, measurements define two frequency intervals at slightly different temperatures (Fig. 10). In LT peridotites, the two frequency intervals range from -37.5 to -12°C and from 20 to 31°C, respectively (Fig. 10a). In HT peridotites, the first ThL distribution interval occurs at slightly higher temperatures, from -24 to 0°C, while the latter occurs in the same interval from 20 to 31 °C (Fig. 10b). Corresponding CO<sub>2</sub> density values range between 1.11 and 1 ± 0.01 g/cm<sup>3</sup> and 0.75 and 0.65 ± 0.01 g/cm<sup>3</sup> in LT peridotites, and between 1.04 and 0.91 ± 0.01 g/cm<sup>3</sup> and 0.75 and 0.65 ± 0.01 g/cm<sup>3</sup> in HT peridotites.

355 As a general rule of thumb, the preservation of fluid inclusion depends on both  
356 inclusion size and on the mechanical properties of the enclosing mineral (e.g. Bodnar et al.  
357 1989; Campione et al. 2015). For this reason, the distribution of ThL measurements for Type  
358 II CO<sub>2</sub> inclusions has also been investigated in the different mineral phases. As shown by the  
359 histograms in Figure 11, ThL distribution is similar in orthopyroxene and clinopyroxene  
360 where the lowest ThL values correspond to a density of  $1.11 \pm 0.1 \text{ g/cm}^3$ . Conversely, in  
361 olivine, ThL's are systematically higher, resulting in lower CO<sub>2</sub> densities not exceeding  $1 \pm$   
362  $0.1 \text{ g/cm}^3$ . Therefore, measured Type II inclusions in olivine have not preserved fluid density  
363 at trapping P-T conditions.

364 To test if partial decrepitation and/or stretching in olivine was dependent on inclusion  
365 size, the densities of 37 inclusions with length  $\leq 3 \text{ }\mu\text{m}$  have been calculated by applying the  
366 Raman densimeter of Kawakami et al. (2003). In Raman spectra, measured distances of the  
367 CO<sub>2</sub> Fermi doublet ( $\Delta$ ) from 105.17 to  $104.46 \pm 0.03 \text{ cm}^{-1}$  correspond to CO<sub>2</sub> densities  
368 between 1.11 to  $0.85 \pm 0.1 \text{ g/cm}^3$  (Fig. 12a). This density interval is similar to that obtained by  
369 microthermometry in larger CO<sub>2</sub> inclusions in orthopyroxene and clinopyroxene (Fig. 12a).  
370 Thus, data indicate a greater tendency to decrepitation of fluid inclusions in olivine than in  
371 pyroxenes, probably due to mechanical failure on decompression from mantle depths.

372

## 373 Discussion

374

### 375 Significance of fluid inclusion data

376 In mantle xenoliths, fluid inclusions represent either mantle metasomatic fluids, or  
377 fluids degassed by ascending basaltic magmas (cf., Andersen and Neumann 2001; Frezzotti

378 and Touret 2014, and references therein). The chemical composition and the density of  
379 metasomatic and magmatic fluids can be different, since trapping can occurs at various  
380 pressure and temperature conditions. Therefore, the chemical composition and the density  
381 distribution of fluid inclusions potentially provide plentiful information on the depths of origin  
382 of mantle rocks, and/or on the episodes of rest magma at confined depths (c.f., Andersen and  
383 Neumann 2001; Frezzotti and Peccerillo 2004; Hansteen and Klügel 2008).

384 The reliability of fluid inclusions as geobarometers relies on the isochoric principle,  
385 governed by the fluid equation of state (Roedder 1965). At trapping P-T conditions, the  
386 pressure of the fluid inside the inclusions equals the lithostatic pressure. During magma  
387 transport, however, the fluid develops relevant overpressures, since the external lithostatic or  
388 magmatic pressure becomes progressively lower than the internal fluid pressure (Roedder  
389 1984). If fluid overpressure exceeds the mechanical strength of the enclosing mineral, fluid  
390 inclusions undergo decrepitation and stretching, with a partial-to-complete fluid loss, resulting  
391 in a density decrease. Inclusion decrepitation and stretching depend on many variables, such  
392 as the composition, size and distribution of the fluid inclusions, and the mechanical strength of  
393 the host mineral (e.g., Bodnar et al. 1989; Vityk and Bodnar 1998; Frezzotti and Viti 2001;  
394 Campione et al. 2015), but it does not reflect a decrease in magma decompression rates. A  
395 slowing down of the ascent rate of magmas - which corresponds to magma rest episodes at  
396 confined depths - can be proposed if decrepitation and stretching reset inclusion densities to  
397 newly-defined lower-pressure intervals and new episodes of fluid trapping occur (cf.,  
398 Andersen and Neumann 2001; Frezzotti and Peccerillo 2004; Hansteen and Klügel 2008).

399 The present study reveals trapping of fluids during subsequent events. Type I  
400 inclusions represent the earlier and deeper fluids, as indicated by their distribution as small  
401 clusters or as crystallographically oriented groups in Ol I and exsolved Opx I of LT  
402 peridotites. Type I fluids are CO<sub>2</sub>-rich and contain variable amounts of N<sub>2</sub>, reaching 18 mol%

403 in the densest inclusion ( $1.19 \text{ g/cm}^3$ ). Their association with  $\text{CO}_2\text{-N}_2$  inclusions containing  
404 carbonates, sulfates,  $\pm$  chlorides and spinel, and with carbonate-silicate glass micro-veins  
405 suggest an origin by immiscibility processes from an original volatile-rich carbonate-silicate  
406 melt in the lithospheric mantle.

407 In the Canary Islands, mantle metasomatism by carbonatitic or carbonate-silicate  
408 melts, enriched in volatiles and incompatible trace elements, was previously described. In  
409 particular, carbonate-rich hydrous fluids or melts were reported in peridotites from Tenerife,  
410 Lanzarote, and La Gomera (Frezzotti et al. 2002a, b; Neumann et al. 1995; 2002; 2004).  
411 Likewise,  $\text{N}_2$  in  $\text{CO}_2$  mantle fluids was reported in peridotites from Lanzarote (Andersen et al.  
412 1995). Notably, the presence of  $\text{N}_2$  in  $\text{CO}_2$ -rich inclusions was also in this case revealed by  
413 Raman microspectroscopy, being Raman the only analytical technique able to detect trace  
414 amounts ( $\leq 0.1 \text{ mol\%}$ ) of  $\text{N}_2$  in fluid inclusions of small size. Metasomatic processes predate  
415 the onset of Canary magmatism (Neumann et al. 2004) and are unrelated to the ascent history  
416 of peridotites in the host lavas.

417 At a later stage, ingress of lower-density  $\text{CO}_2$  fluids occurred in both LT and HT  
418 peridotites. Type II inclusion distribution along intergranular trails is suggestive of fluid  
419 trapping by micro-fracturing of peridotites.  $\text{CO}_2$  density distribution intervals suggest two  
420 distinct fluid trapping and re-equilibration events (Fig. 10). In LT peridotites ( $T = 800 -$   
421  $950^\circ\text{C}$ ), density intervals are from  $1.11$  to  $0.99 \pm 0.01 \text{ g/cm}^3$  and from  $0.75$  to  $0.65 \pm 0.01$   
422  $\text{g/cm}^3$ , respectively (Fig. 12a). In peridotites equilibrated at higher temperatures (HT  
423 peridotites;  $T = 900\text{-}1100^\circ\text{C}$ ),  $\text{CO}_2$  density distribution shows similar, although slightly lower,  
424 values from  $1.04$  to  $0.91 \pm 0.01 \text{ g/cm}^3$  and from  $0.75$  to  $0.65 \pm 0.01 \text{ g/cm}^3$ , respectively (Fig.  
425 12b).

426           The clear-cut variation of the chemistry of Type II inclusions, which consist of pure  
427 CO<sub>2</sub>, suggests a different fluid origin, probably by degassing of magmas. Canary alkaline  
428 mafic magmas are carbon-rich and thus can begin to exsolve CO<sub>2</sub>-rich fluids at great pressures  
429 (> 1 GPa; Longpré et al. 2017) in the oceanic lithospheric mantle.

430

#### 431 Fluid inclusions geothermobarometry

432           Once the composition and density of the fluids are defined, temperatures be known in  
433 order to calculate pressure conditions by fluid equations of state (Roedder 1965; 1984). In  
434 general, the temperature of the host lavas is taken as representative of fluid trapping conditions  
435 in mantle xenoliths (cf., Andersen and Neumann 2001; Hansteen and Klügel 2008). In the  
436 present case, however, the preservation of Type I inclusions only in LT peridotites, and the  
437 density differences of Type II CO<sub>2</sub> fluids in LT and HT peridotites suggest that xenoliths did  
438 not reach the same temperatures during ascent. For this reason, fluid trapping temperatures  
439 have been assumed based on mantle mineral geothermometry: 800 - 950°C for LT peridotites,  
440 and 900 - 1100°C for HT peridotites (Wells 1977, Brey and Koehler 1990 and Witt-Eickschen  
441 and Seck 1991). From each temperature interval, the highest value has been selected assuming  
442 the presence of a component of increasing temperature caused by the ascent of mantle  
443 xenoliths in the basaltic host lavas.

444           The P-T distribution of Type I and II fluid isochores is reported in Figure 13. The  
445 extremely high densities of Type I CO<sub>2</sub>-N<sub>2</sub> fluids in LT peridotites (1.19 g/cm<sup>3</sup>; inclusion S4),  
446 correspond to trapping pressures of  $1.8 \pm 0.02$  GPa at 950°C (gray star in Fig. 13). This  
447 pressure is consistent with mineral geobarometry data, which indicate equilibration of  
448 peridotites in the mantle at 1.5 - 2.0 GPa for the same temperatures (Koehler and Brey 1990).

449           Conversely, trapping and/or re-equilibration of Type II CO<sub>2</sub> fluids occurred at lower  
450 pressures (Fig. 13) during two distinct episodes of magma rest at confined depths. In LT  
451 peridotites, isochore distribution for the denser Type II inclusions correspond to pressures  
452 comprised from 1 to  $0.67 \pm 0.02$  GPa, at 950°C (green band in Fig. 13). In HT peridotites,  
453 Type II fluid isochores indicate similar, though slightly lower, pressures from 0.89 to  $0.60 \pm$   
454  $0.02$  GPa at 1100 °C (blue band in Fig. 13). As illustrated in the P-T diagram in Figure 13,  
455 largely overlapping isochoric bands confirm that Type II inclusions in both LT and HT  
456 peridotites record a common deep magma storage region. The somewhat higher pressure  
457 values calculated for Type II fluids in LT rocks (Fig. 13) put forward that fluid inclusions are  
458 better preserved in rocks equilibrated at lower temperatures.

459           A second CO<sub>2</sub> trapping and re-equilibration event is defined by isochoric pressures  
460 (red isochore bands in Fig. 13) from 0.34 to  $0.26 \pm 0.02$  GPa at 950°C (Type II inclusions in  
461 LT peridotites) and from 0.36 to  $0.28 \pm 0.02$  GPa at 1100°C (Type II inclusions in HT  
462 peridotites). In HT and LT peridotites, the isochore bands for Type II inclusions differ from  
463 each other of only 0.02 GPa. This negligible pressure variation confirms the accuracy of  
464 pressure estimates. This fluid trapping event corresponds to the last episode of magma rest  
465 before eruption.

466

#### 467 Recent magma transport dynamics beneath El Hierro

468           In order to model magma transport dynamics beneath El Hierro, once having found the  
469 P-T conditions for fluid trapping, we have to define the corresponding depths. Fluid isochoric  
470 pressures have been converted into depths following the relation:  $h = P/(g \cdot d)$ , where h is the  
471 depth of origin or trapping of the fluids, P the lithostatic pressure, g the acceleration of gravity  
472 ( $9.81 \text{ m/sec}^2$ ), and d the density of column-rocks. Main rock layer densities have been defined

473 based on the following simplified stratigraphic reconstruction: a sequence of volcanic products  
474 and rocks with a density of  $2.5 \text{ g/cm}^3$  for the volcanic edifice (emergent and submarine height  
475 of island of about 4500 m; Acosta et al. 2005; Carracedo et al. 2012), a basaltic oceanic crust  
476 with a density of  $2.7 \text{ g/cm}^3$  (about 8500 m), and lithospheric peridotites with a density of  $3.3$   
477  $\text{g/cm}^3$ .

478 Fluid inclusions studies in peridotite xenoliths allow concluding that polybaric magma  
479 transport characterizes the Rift Volcanism activity at about 40-30 ka. The resulting model is  
480 illustrated schematically in Figure 14 and discussed in the following sections.

481 El Hierro volcano is built on oceanic crust extending to about 12 - 15 km (Martinez et  
482 al. 2013) of a thick lithosphere of about 90 - 95 km (Dasgupta et al. 2010). Type I  $\text{CO}_2\text{-N}_2$   
483 fluids associated with carbonate-silicate melts indicate that peridotites erupted from a source  
484 within the depth range of 60-65 km ( $P = 1.80 \pm 0.02 \text{ GPa}$ ; gray star in Fig. 14) in the lower  
485 lithospheric mantle. As discussed in the previous sections, geochemical characteristics of  
486 peridotites beneath the Canary islands point to mantle metasomatism by carbonate-rich melts  
487 (e.g. Neumann 2004). The presence of oceanic carbonatites of Oligocene to Lower Miocene  
488 age in Fuerteventura (Lebas et al. 1986) provides further support to a carbonate enriched  
489 lithosphere.

490 Type II fluid inclusions have been trapped during magma rest at confined depths for a  
491 time sufficient to allow  $\text{CO}_2$  trapping. Fluid density distribution identifies two main magma  
492 accumulation regions. The deeper one is located in the shallow lithospheric mantle at depths  
493 comprised from 37 to 22 km (Fig. 14). This mantle magma reservoir served as the main  
494 storage volume of the volcano and fed a smaller reservoir at 10 - 12 km depth (Fig. 14) near  
495 the base of the oceanic crust, from where mafic magmas erupted.

496 Magma storage at crustal conditions does not appear to be long-lived. The preservation  
497 of high-density Type I and II inclusions suggests that mafic magmas arrived into the lower  
498 oceanic crust shortly before (e.g. day timescale) the eruption. Longer magma stagnation would  
499 have caused the complete resetting of fluid inclusion densities to shallower ambient pressures  
500 (Wanamaker and Evans 1989; Hansteen and Klügel 2008).

501 The lithospheric mantle reservoir revealed by present study is particularly thick, on the  
502 order of 15 km (i.e. from 37 to 22 km depth). Thus, magma is likely to have been stored in a  
503 series of interconnected pockets distributed over this wide depth interval (Fig. 14). Similar  
504 magma accumulation as vertically-stacked small reservoirs has been previously characterized  
505 for Kilauea and Piton de la Fournaise (Decker 1987; Ryan et al. 1988; Voogd et al. 1999;  
506 Michon et al. 2015). In these volcanoes, deep magma transport dynamics has been interpreted  
507 as the result of magma storage in the lithospheric mantle, either through a micro-fracture  
508 network system over a wide depth interval (e.g. magma-fracking by CO<sub>2</sub> degassing; Shaw et  
509 al. 1980; Pollard et al. 1983; Decker 1987), or in a porous mantle matrix (Gudmundsson  
510 1987). Partially molten mantle storage regions where magma rest and degas are considered to  
511 be long-lived (Shaw et al. 1980; Pollard et al. 1983; Decker 1987); although their formation is  
512 still not unanimously accepted, they have been proposed in regions of oceanic intraplate  
513 volcanism characterized by slow magma supply (e.g. Shaw et al. 1980), which would be in  
514 agreement with the low long-term magma rate of El Hierro volcano (0.12-0.13 km<sup>3</sup>/ka;  
515 Carracedo 1999).

516 The proposed polybaric magma storage system appears to agree with magma transport  
517 dynamics reconstructed for the 2011-2012 eruption (e.g., Meletlidis et al. 2012; Becerill et al.  
518 2013b; González et al., 2013; Martí et al. 2013; Longpré et al. 2014; Klügel et al. 2015).  
519 Therefore, it seems that the magma plumbing system has been essentially the same for the last  
520 30–40 ka. For instance, the upper limit of the deep magma storage region identified by fluid



521 inclusions at approximately 22 km (Fig. 14) corresponds to the depth of the pre- sin-eruptive  
522 earthquake hypocenters (20 - 25 km) interpreted to reflect the magma source that fed the  
523 2011-2012 eruption (e.g. López et al. 2012; Martí et al. 2013; Longpré et al. 2014).  
524 Furthermore, storage of 2011-2012 magma in the lower oceanic crust is likewise considered  
525 ephemeral, not developing into a long-term reservoir (e.g., Becceril et al. 2013b; Longpré et  
526 al. 2014; Martí et al. 2013; Klügel et al. 2015). These Authors further interpreted the pre-  
527 eruptive lateral magma migration of about 15–20 km from north to south as evidence of sill  
528 propagation. Although fluid inclusion data cannot resolve horizontal magma movements,  
529 temporary magma stagnation in a region of neutral buoyancy, such as the lower crust, might  
530 have favored lateral transport.

531 In oceanic islands, magma pathways are established in the early growth stages but  
532 evolve on time, along with the volcano. Our model does not indicate storage of magmas  
533 directly beneath the Moho (i.e., 15 to 25 km) for present rift volcanism activity, as previously  
534 proposed by Stroncik et al. (2009) based on clinopyroxene-melt geobarometric data in  
535 prehistorical lavas of undetermined age. Confinement of magmas at about 7-10 km below the  
536 geophysical interface of the oceanic crust and the mantle (12 - 15 km; Fig. 14) can be  
537 tentatively interpreted as an indication of magma underplating below El Hierro. At the nearby  
538 island of La Palma, progressive deepening of the magma plumbing system, induced by up to  
539 10 km magma underplating, has been recently proposed by Barker et al. (2015). Similarly,  
540 geophysical data from the Canary Islands (Carracedo et al. 2015) point to underplating  
541 beneath Tenerife and Gran Canaria over the same depth interval. In this respect, further studies  
542 of fluid inclusions in mantle xenoliths in lavas of older volcanic cycles of El Hierro should  
543 make it possible to trace the evolution of magma transport beneath this volcano over its entire  
544 history.

545

## 546    **Summary and Conclusions**

547

548        Present study focuses on the reconstruction of a model for the recent magma dynamics  
549    beneath El Hierro Island based on combined fluid inclusion and mineral geothermobarometry  
550    in mantle xenoliths entrained in lavas of the Rift Volcanism activity (40-30 ka). Two distinct  
551    fluid phases have been characterized by microthermometry and Raman microspectroscopy.  
552    Type I CO<sub>2</sub>-N<sub>2</sub> mantle metasomatic fluids are trapped at pressure of  $1.80 \pm 0.02$  GPa, or about  
553    60-65 km depth, before xenolith entrainment in the host lava. Type II CO<sub>2</sub> fluids, probably  
554    degassed from host mafic magmas, reveal two discrete magma accumulation regions: the first  
555    in the lithospheric mantle, from 1 to  $0.60 \pm 0.02$  GPa, or 37 to 22 km depth, and the latter in  
556    the lower oceanic crust, from 0.34 to  $0.21 \pm 0.02$  GPa, or 12 to 10 km depth,. The deeper  
557    accumulation region is interpreted as a stacked system of interconnected small magma pockets  
558    distributed in the lithospheric mantle beneath the Island, which fed a temporary lower crustal  
559    storage region.

560        Models of the internal structure of active volcanoes are important for constraining  
561    reliable monitoring strategies and forecasting volcanic eruptions. Present fluid inclusion study  
562    can probably produce a reliable model on how El Hierro volcano works, since magma  
563    migration within the plumbing system is comparable to that registered during the 2011-2012  
564    eruption. The implications are that magma migration from the deep reservoir should be  
565    monitored as precursor of magma rise and hence eruption, by considering both mantle  
566    seismicity, conceivably connected with upward migration of earthquake hypocenters, and  
567    changes in the gravity field as a consequence of magma migration within the plumbing  
568    system.

569

## 570 Acknowledgements

571

572 This paper is a part of E.O. Ph.D. thesis. We are grateful to L. Becceril, M. Campione,  
573 F. Lucchi, N. Malaspina, and V. Zanon for helpful discussions. We acknowledge A.  
574 Risplendente for assistance during microprobe analyses. Editorial handling by V. Kamenetsky,  
575 and reviews by F. Deegan, T. Hansteen and an anonymous reviewer have considerably  
576 improved the manuscript. Funding was provided by the University of Milan Bicocca, FAR-  
577 2015 to M.L.F and I.M.V.. Raman facilities were provided by the Interdepartmental Center  
578 "G. Scansetti" for studies on asbestos and other toxic particulates at the University of Turin.

579

580

581

## 582 References

583

- 584 Acosta J, Uchupi E, Muñoz A, Herranz P, Palomo C, Ballesteros M, Working ZE (2005)  
585 Geologic evolution of the Canarian Islands of Lanzarote, Fuerteventura, Gran Canaria and  
586 La Gomera and comparison of landslides at these islands with those at Tenerife, La Palma  
587 and El Hierro. *Mar Geophys Res* 24:1–40
- 588 Andersen T, Burke EJ, Neumann ER (1995) Nitrogen-rich fluid in the upper mantle: fluid  
589 inclusions in spinel dunite from Lanzarote, Canary Islands. *Contrib Mineral Petrol*  
590 120:20–28
- 591 Andersen T, Neumann ER (2001) Fluid inclusions in mantle xenoliths. *Lithos* 55:301–32.
- 592 Anguita F, Hernan F (1975) A propagating fracture model versus a hot spot origin for the  
593 Canary Islands. *Earth Planet Sci Lett* 27:11–19
- 594 Anguita F, Hernán F (2000) The Canary Islands origin: a unifying model. *J Volcanol and*  
595 *Geotherm Res* 103:1–26. [http://doi/10.1016/S0377-0273\(00\)00195-5](http://doi/10.1016/S0377-0273(00)00195-5)
- 596 Araña V, Ortiz R (1991) The Canary Islands: tectonics, magmatism and geodynamic  
597 framework. In: A. Kampunzu, R. Lubala (eds) *Magmatism in Extensional Structures*  
598 *Setting: The Phanerozoic African Plate*, Springer Verlag, pp. 209–249
- 599 Bakker RJ (2003) Package FLUIDS1. Computer programs for analysis of fluid inclusion data  
600 and for modelling bulk fluid properties. *Chem Geol* 194:3–23

601 Barker AK, Troll VR, Carracedo JC, Nicholls PA (2015) The magma plumbing system for the  
602 1971 Teneguía eruption on La Palma, Canary Islands. *Contrib Mineral Petrol* 170:5–6

603 Becerril L, Cappello A, Galindo I, Neri M, Del Negro C (2013a) Spatial probability  
604 distribution of future volcanic eruptions at El Hierro Island (Canary Islands, Spain). *J*  
605 *Volcanol Geotherm Res* 257:21–30

606 Becerril L, Galindo I, Gudmundsson A, Morales JM (2013b) Depth of origin of magma in  
607 eruptions. *Sci Rep* 3:1–6. <http://doi.org/10.1038/srep02762>

608 Becerril L, Galindo I, Martí J, Gudmundsson A (2015) Three-armed rifts or masked radial  
609 pattern of eruptive fissures? The intriguing case of El Hierro volcano (Canary Islands).  
610 *Tectonophysics* 647:33–47

611 Bertagnini A, Métrich N, Landi P, Rosi M (2003) Stromboli volcano (Aeolian Archipelago,  
612 Italy): an open window on the deep-feeding system of a steady state basaltic volcano. *J*  
613 *Geophys Res* 108: 2336–2342

614 Bodnar RJ (2003) Introduction to aqueous-electrolyte fluid inclusions. *Fluid Inclusions:*  
615 *Analysis and Interpretation*. In I. Samson, A. Anderson, D. Marshall (eds) Mineral Assoc  
616 Canada, Short Course 32, pp. 81–100

617 Bodnar RJ, Binns PR, Hall DL (1989) Synthetic fluid inclusions-VI. Quantitative evaluation  
618 of the decrepitation behaviour of fluid inclusions in quartz at one atmosphere confining  
619 pressure. *J Metam Geol* 7:229–242

620 Brey GP, Köhler T (1990) Geothermobarometry in four-phase lherzolites II. New  
621 thermobarometers, and practical assessment of existing thermobarometers. *J Petrol*  
622 31:1353–1378

623 Campione M, Malaspina N, Frezzotti ML (2015) Threshold size for fluid inclusion  
624 decrepitation. *J Geophys Res Solid Earth* 120:7396–7402

625 Carracedo JC (1994). The Canary Islands: an example of structural control on the growth of  
626 large ocean-island volcanoes. *J Volcanol Geotherm Res* 60:225–241

627 Carracedo JC (1999) Growth, structure, instability and collapse of Canarian volcanoes and  
628 comparisons with Hawaiian volcanoes. *J Volcanol Geotherm Res* 94:1–19

629 Carracedo JC, Day S, Guillou H, Rodríguez Badiola E, Canas JA, Pérez Torrado FJ (1998)  
630 Hotspot volcanism close to a passive continental margin: the Canary Islands. *Geol Mag*  
631 135: 591–604

632 Carracedo JC, Badiola ER, Guillou H, de La Nuez J, Pérez Torrado FJ (2001) Geology and  
633 volcanology of La Palma and El Hierro (Canary Islands). *Estudios Geol* 57:175–273

634 Carracedo JC, Perez-Torrado FJ, Rodriguez-Gonzalez A, Fernandez-Turiel JL, Klügel A,  
635 Troll, VR, Wiesmaier S (2012) The ongoing volcanic eruption of El Hierro, Canary  
636 Islands. *Eos* 93: 89–90

637 Carracedo JC., Troll VR, Zaczek K, Rodriguez-Gonzalez A, Soler V, Deegan FM (2015) The  
638 2011–2012 submarine eruption off El Hierro, Canary Islands: New lessons in oceanic  
639 island growth and volcanic crisis management. *Earth-Sci Rev* 150:168–200

640 Dasgupta R, Jackson MG, Lee C-TA (2010) Major element chemistry of ocean island basalts -  
641 Conditions of mantle melting and heterogeneity of mantle source. *Earth Planet Sci Lett*  
642 289:377–392

643 De Vivo B, Frezzotti ML, Lima A, Trigila R (1988) Spinel lherzolite nodules from Oahu  
644 Island (Hawaii): a fluid inclusion study. *Bull Mineral* 111:307–319

645 Decker RW, Wright TL, Stauffer, S (1987). *Volcanism in Hawaii*. US Government Printing  
646 Office, p 1606

647 Duggen S, Hoernle K, Hauff F, Klügel, A, Bouabdellah M, Thirlwall MF (2009) Flow of  
648 Canary mantle plume material through a subcontinental lithospheric corridor beneath  
649 Africa to the Mediterranean. *Geology* 37:283–286

650 Duschek W, Kleinrahm R, Wagner W (1990) Measurement and correlation of the (pressure,  
651 density, temperature) relation of carbon dioxide I. The homogeneous gas and liquid  
652 regions in the temperature range from 217 K to 340 K at pressures up to 9 MPa. *J Chem*  
653 *Thermodyn* 22:827–840. [http://doi.org/10.1016/0021-9614\(90\)90172-M](http://doi.org/10.1016/0021-9614(90)90172-M)

654 Frey FA, Prinz M (1978) Ultramafic inclusions from San Carlos, Arizona: petrologic and  
655 geochemical data bearing on their petrogenesis. *Earth Planet Sci Lett* 38:129–176

656 Frezzotti ML, Peccerillo A (2004) Fluid inclusion and petrological studies elucidate  
657 reconstruction of magma conduits. *Eos* 85:157–160

658 Frezzotti ML, Touret JL (2014) CO<sub>2</sub>, carbonate-rich melts, and brines in the mantle. *Geosci*  
659 *Front* 5:697–710

660 Frezzotti ML, De Vivo B, Clocchiatti R (1991) Melt-mineral-fluid interactions in ultramafic  
661 nodules from alkaline lavas of Mount Etna (Sicily, Italy): melt and fluid inclusion  
662 evidence. *J Volcanol Geotherm Res* 47:209–219

663 Frezzotti ML, Touret JL, Lustenhouwer WJ, Neumann ER (1994) Melt and fluid inclusions in  
664 dunite xenoliths from La Gomera, Canary Islands: tracking the mantle metasomatic fluids.  
665 *Eur J Mineral* 6:805–817

666 Frezzotti ML, Andersen T, Neumann ER, Simonsen SL (2002a) Carbonatite melt–CO<sub>2</sub> fluid  
667 inclusions in mantle xenoliths from Tenerife, Canary Islands: a story of trapping,  
668 immiscibility and fluid–rock interaction in the upper mantle. *Lithos* 64:77–96

669 Frezzotti ML, Touret JL, Neumann ER (2002b) Ephemeral carbonate melts in the upper  
670 mantle. *Eur J Mineral* 14:891–904

671 Frezzotti ML, Tecce F, Casagli A (2012) Raman spectroscopy for fluid inclusion analysis. *J*  
672 *Geochem Explor* 112:1–20

673 Füster J (1975) Las Islas Canarias: un ejemplo de evolución temporal y espacial del  
674 vulcanismo oceánico. *Est Geol* 31: 439–463

675 Garrabos Y, Tufeu R, Le Neindre B, Zalczer G, Beysens D (1980) Rayleigh and Raman  
676 scattering near the critical point of carbon dioxide. *J Chem Phys* 72:4637–4651

677 Gee MJR, Masson DG, Watts AB, Mitchell NC (2001) Offshore continuation of volcanic rift  
678 zones, El Hierro, Canary Islands. *J Volcanol Geother Res* 105:107–119

679 Geyer A, Martí J (2010) Tectonophysics The distribution of basaltic volcanism on Tenerife,  
680 Canary Islands: Implications on the origin and dynamics of the rift systems.  
681 *Tectonophysics* 483: 310–326

682 González PJ, Samsonov SV, Pepe S, Tiampo KF, Tizzani P, Casu F, Sansosti E (2013)  
683 Magma storage and migration associated with the 2011 – 2012 El Hierro eruption:  
684 Implications for crustal magmatic systems at oceanic island volcanoes, *J Geophys Res*  
685 *Solid Earth* 118:4361–4377

686 Gudmundsson A (1987) Geometry, formation and development of tectonic fractures on the  
687 Reykjanes Peninsula, southwest Iceland. *Tectonophysics* 139: 295–308

688 Guillou H, Carracedo JC, Torrado FP, Badiola ER (1996) K-Ar ages and magnetic  
689 stratigraphy of a hotspot-induced, fast grown oceanic island: El Hierro, Canary Islands. *J*  
690 *Volcanol Geother Res* 73:141–155

691 Hansteen TH, Klügel A, (2008) Fluid inclusion thermobarometry as a tracer for magmatic  
692 processes. In: Putirka KD, Tepley FJ (eds) *Reviews in Mineralogy Min Soc Amer*  
693 149:143–177

694 Hansteen TH, Andersen T, Neumann ER, Jelsma H (1991) Fluid and silicate glass inclusions  
695 in ultramafic and mafic xenoliths from Hierro, Canary Islands: implications for mantle  
696 metasomatism. *Contrib Mineral Petrol* 107:242–254

697 Hansteen TH, Klügel A, Schmincke HU (1998) Multi-stage magma ascent beneath the Canary  
698 Islands: evidence from fluid inclusions. *Contrib Mineral Petrol* 132:48–64

699 Hoernle K, Schmincke HU (1993) The Role of Partial Melting in the 15-Ma Geochemical  
700 Evolution of Gran Canaria: A Blob Model for the Canary Hotspot, *J Petrol* 34:599–626

701 Hoernle KAJ (1998) Geochemistry of Jurassic oceanic crust beneath Gran Canaria (Canary  
702 Islands): implications for crustal recycling and assimilation. *J Petrol* 39:859–880

703 Holloway JR (1977). Fugacity and activity of molecular species in supercritical fluids. In: DG  
704 Fraser (ed) in *Thermodynamics in Geology*, Dordrecht-Holland, pp. 161–181

705 Holloway JR (1981) Compositions and volumes of supercritical fluids. In: L Hollister, ML  
706 Crawford (eds) *Fluid inclusions: application to petrology*, Short Course Handbook, pp. 13-  
707 38

708 IGME (2010a) Mapa Geológico de España, Escala 1:25.000. Isla de El Hierro. Hoja 1105- II,  
709 Valverde, pp, 96

710 IGME (2010b) Mapa Geológico de España, Escala 1:25.000. Isla de El Hierro. Hoja 1105- III,  
711 Sabinosa, pp, 71

712 IGME (2010c) Mapa Geológico de España, Escala 1:25.000. Isla de El Hierro. Hoja 1105- IV,  
713 Frontera, pp, 84

- 714 IGME (2010d) Mapa Geológico de España, Escala 1:25.000. Isla de El Hierro. Hoja 1108-  
715 I/II, La Restinga, pp, 55
- 716 Kawakami Y, Yamamoto J, Kagi H (2003) Micro-Raman Densimeter for CO<sub>2</sub> Inclusions in  
717 Mantle-Derived Minerals. *Applied Spectrosc* 57:1333–1339
- 718 Klemm R, van den Kerkhof, AM, Horn EE (1992) High-density CO<sub>2</sub> – N<sub>2</sub> inclusions in  
719 eclogite-facies metasediments of the Münchberg gneiss complex, SE Germany. *Contrib*  
720 *Mineral Petrol* 111:409–419
- 721 Klügel A, Hansteen TH, Galipp K (2005) Magma storage and underplating beneath Cumbre  
722 Vieja volcano, La Palma (Canary Islands). *Earth Planet Sci Lett* 236:211–226
- 723 Klügel A, Longpré MA, García-Cañada L, Stix J, (2015) Deep intrusions, lateral magma  
724 transport and related uplift at ocean island volcanoes. *Earth Planet Sci Lett* 43:140–149
- 725 Koehler TP, Brey GP, (1990) Calcium exchange between olivine and clinopyroxene calibrated  
726 as a geothermobarometer for natural peridotites from 2 to 60 kb with applications.  
727 *Geochim Cosmochim Acta* 54:2375–2388
- 728 Lebas MJ, Rex DC, Stillman CJ (1986) The early magmatic chronology of Fuerteventura,  
729 Canary Islands. *Geol Mag* 123: 287–298
- 730 Longpré MA, Chadwick JP, Wijbrans J, Iping R (2011) Age of the El Golfo debris avalanche,  
731 El Hierro (Canary Islands): New constraints from laser and furnace <sup>40</sup>Ar/ <sup>39</sup>Ar dating. *J*  
732 *Volcanol Geother Res* 203:76–80
- 733 Longpré MA, Klügel A, Diehl A, Stix J (2014) Mixing in mantle magma reservoirs prior to  
734 and during the 2011 – 2012 eruption at El Hierro, Canary Islands. *Geology* 42:315–318
- 735 Longpré MA, Stix J, Klügel A, Shimizu N (2017) Mantle to surface degassing of carbon-and  
736 sulphur-rich alkaline magma at El Hierro, Canary Islands. *Earth Planet Sci Lett* 460:268-  
737 280
- 738 López C, Blanco MJ, Abella R, Brenes B, Cabrera Rodríguez VM, Casas B, Domínguez  
739 Cerdeña I, Felpeto A, Fernández de Villalta M, del Fresno C, García O, García-Arias MJ,  
740 García-Cañada L, Gomis Moreno A, González-Alonso E, Guzmán Pérez J, Iribarren F,  
741 López-Díaz R, Luengo-Oroz N, Meletlidis S, Moreno M, Moure D, Pereda de Pablo J,  
742 Rodero E, Romero E, Sainz-Maza S, Sentre Domingo MA, Torres PA, Trigo, P,  
743 Villasante-Marcos V (2012) Monitoring the volcanic unrest of El Hierro (Canary Islands)  
744 before the onset of the 2011–2012 submarine eruption. *Geophys Res Lett* 39 L13303
- 745 Lustrino M, Wilson M (2007) The circum-Mediterranean anorogenic Cenozoic igneous  
746 province: *Earth-Sci Rev* 81: 1–65
- 747 Marinoni LB, Pasquaré G (1994) Tectonic evolution of the emergent part of a volcanic ocean  
748 island: Lanzarote, Canary Islands. *Tectonophysics* 239:111–137
- 749 Marinoni LB, Gudmundsson A (2000) Dykes, faults and palaeostresses in the Teno and Anaga  
750 massifs of Tenerife (Canary Islands). *J Volcanol and Geother Res* 103:83–103

751 Martí J, Pinel V, López C, Geyer A, Abella R, Tárraga M, Rodríguez C (2013a) Causes and  
752 mechanisms of the 2011-2012 El Hierro (Canary Islands) submarine eruption. *J Geophys*  
753 *Res Solid Earth*, 118:823–839

754 Martí J, Castro A, Rodríguez C, Costa F, Carrasquilla S, Pedreira R, Bolos X (2013b)  
755 Correlation of magma evolution and geophysical monitoring during the 2011-2012 El  
756 Hierro (Canary Islands) submarine eruption. *J Petrol* 54:1349–1373

757 Martínez-Arevalo C, Mancilla FD, Helffrich G, García A (2013) Seismic evidence of a  
758 regional sublithospheric low velocity layer beneath the Canary Islands. *Tectonophysics*  
759 608:586–599

760 Masson DG (1996) Catastrophic collapse of the volcanic island of Hierro 15 ka ago and the  
761 history of landslides in the Canary Islands. *Geology* 24: 231–234

762 Masson DG, Watts B, Gee MJR, Urgeles R, Mitchell NC, Le Bas TP, Canals M. (2002) Slope  
763 failures on the flanks of the western Canary Islands. *Earth-Sci Rev* 57:1–35

764 Masson DG, Harbitz CB, Wynn RB, Pedersen G, Løvholt F (2006) Submarine landslides:  
765 processes, triggers and hazard prediction. *Philosophical Transactions. Series A Math*  
766 *Physical Eng Sci* 364:2009–2039

767 Meletlidis S, Roberto A, Di Pompilio M, Bertagnini A, Iribarren I, Felpeto A, Oriano CD  
768 (2012) Xenopumices from the 2011 – 2012 submarine eruption of El Hierro (Canary  
769 Islands, Spain): Constraints on the plumbing system and magma ascent, *Geophys Res Lett*  
770 39:1–6

771 Michon L, Ferrazzini V, Di Muro A, Villeneuve N, Famin V (2015) Rift zones and magma  
772 plumbing system of Piton de la Fournaise volcano: How do they differ from Hawaii and  
773 Etna? *J Volcanol Geother Res* 303:112–129

774 Morgan DJ, Jerram DA, Chertkoff DG, Davidson JP, Pearson DG, Kronz A, Nowell GM  
775 (2007) Combining CSD and isotopic microanalysis: Magma supply and mixing processes  
776 at Stromboli Volcano, Aeolian Islands, Italy. *Earth Planet Sci Lett* 260:419–431

777 Neumann E (1990) Ultramafic and mafic xenoliths from Hierro, Canary Islands: evidence for  
778 melt infiltration in the upper mantle. *J Chem* 53:1689–1699

779 Neumann ER, Wulff-Pedersen E, Johnsen K, Andersen T, Krogh E (1995) Petrogenesis of  
780 spinel harzburgite and dunite suite xenoliths from Lanzarote, eastern Canary Islands:  
781 Implications for the upper mantle. *Lithos* 35:83–107

782 Neumann ER, Wulff-Pedersen E, Pearson NJ, Spencer EA (2002) Mantle Xenoliths from  
783 Tenerife (Canary Islands): Evidence for Reactions between Mantle Peridotites and Silicic  
784 Carbonatite Melts inducing Ca Metasomatism. *J Petrol* 43:825–857

785 Neumann ER, Griffin WL, Pearson NJ, O'Reilly SY (2004) The evolution of the upper mantle  
786 beneath the Canary Islands: Information from trace elements and Sr isotope ratios in  
787 minerals in mantle xenoliths. *J Petrol* 45: 2573–2612



788 Pasteris JD, Wopenka B, Seitz JC (1988) Practical aspects of quantitative laser Raman  
789 microprobe spectroscopy for the study of fluid inclusions. *Geochim Cosmochim Acta*  
790 52:979–988

791 Peccerillo A, Frezzotti ML, De Astis G, Ventura G (2006) Modeling the magma plumbing  
792 system of Vulcano (Aeolian Islands, Italy) by integrated fluid-inclusion geobarometry,  
793 petrology, and geophysics. *Geology* 34:17–20

794 Pollard DD, Delaney PT, Duffield WA, Endo ET, Okamura AT (1983) Surface deformation in  
795 volcanic rift zones. *Tectonophysics* 94:541–584

796 Robertson AHF, Stillman CJ (1979) Submarine volcanic and associated sedimentary rocks of  
797 the Fuerteventura Basal Complex, Canary Islands. *Geolog Mag* 116:203–214

798 Roedder E (1965) Liquid CO<sub>2</sub> inclusions in olivine-bearing nodules and phenocrysts from  
799 basalts. *Amer Miner* 50:20–40

800 Roedder, E (1983). Geobarometry of ultramafic xenoliths from Loihi Seamount, Hawaii, on  
801 the basis of CO<sub>2</sub> inclusions in olivine. *Earth Planet Sci Lett* 66:369–379

802 Roedder E (1984) Fluid inclusions. Roedder, E. (1984) Fluid Inclusions. Reviews in  
803 Mineralogy Vol. 12. Mineral Soc Am, pp. 644

804 Rosso KM, Bodnar RJ (1995) Detection limits of CO<sub>2</sub> in fluid inclusions using  
805 microthermometry and laser Raman spectroscopy and the spectroscopic characterization of  
806 CO<sub>2</sub>. *Geochim Cosmochim Acta* 59:3961–3975

807 Ryan MP (1988) Structure of Active Magmatic Systems' Kilauea Volcano, Hawaii. *Journal of*  
808 *Geophys Res* 93(B5): 4213–4248. <http://doi.org/10.1029/JB093iB05p04213>

809 Scandone R, Cashman KV, Malone SD (2007) Magma supply, magma ascent and the style of  
810 volcanic eruptions. *Earth Planet Sci Lett* 253:513–529

811 Schmincke HU (1982) Volcanic and chemical evolution of the Canary Islands. In: U VonRad  
812 et al. (eds) *Geology of the northwest African continental margin*. Springer Verlag, New  
813 York, pp. 273–306

814 Schmincke HU, Sumita M, (1998) Volcanic evolution of Gran Canaria reconstructed from  
815 apron sediments: synthesis of vicap project drilling. *Proceedings of the Ocean Drilling*  
816 *Program, Sci Res* 157:443–469

817 Schwarz S, Klügel A, Wohlgemuth-Ueberwasser C (2004) Melt extraction pathways and  
818 stagnation depths beneath the Madeira and Desertas rift zones (NE Atlantic) inferred from  
819 barometric studies. *Contrib Mineral Petrol* 147:228–240

820 Shaw HR (1980) The fracture mechanisms of magma transport from the mantle to the surface.  
821 *Phys Magmat Processes* 64:201–264

822 Sparks RSJ (2003) Forecasting volcanic eruptions. *Earth Planet Sci Lett* 210:1–15

823 Stronck NA, Klügel A, Hansteen TH (2009) The magmatic plumbing system beneath El  
824 Hierro (Canary Islands): constraints from phenocrysts and naturally quenched basaltic  
825 glasses in submarine rocks. *Contrib Mineral Petrol* 157:165

- 826 Ulmer P (1986) NORM-Program for cation and oxygen mineral norms. Computer Library,  
827 Institut für Mineralogie und Petrographie, ETH-Zentrum, Zürich, Switzerland.
- 828 van den Kerkhof AM (1988) The system CO<sub>2</sub>–CH<sub>4</sub>–N<sub>2</sub> in fluid inclusions: theoretical  
829 modelling and geological applications. PhD Dissertation, Amsterdam Free University, pp.  
830 206
- 831 Viti C, Frezzotti ML (2000) Re-equilibration of glass and CO<sub>2</sub> inclusions in xenolith olivine:  
832 A TEM study. *Amer Mineral* 85:1390-1396
- 833 Viti C, Frezzotti ML (2001) Transmission electron microscopy applied to fluid inclusion  
834 investigations. *Lithos* 55:125–138
- 835 Vityk MO, Bodnar R J (1998) Statistical microthermometry of synthetic fluid inclusions in  
836 quartz during decompression re-equilibration. *Contrib Mineral Petrol* 132:149-162
- 837 Voog DB, Palomé SP, Hirn A, Charvis P, Gallart J, Rousset D, Perroud H (1999) Vertical  
838 movements and material transport during hotspot activity: Seismic reflection profiling  
839 offshore La Réunion. *J Geophys Res* 104:2855-2874
- 840 Wanamaker B.J, Evans B (1989) Mechanical re-equilibration of fluid inclusions in San Carlos  
841 olivine by power-law creep. *Contrib Mineral Petrol* 102:102-111
- 842 Wang CH, Wright RB (1973) Effect of density on the Raman scattering of molecular fluids. I.  
843 A detailed study of the scattering polarization, intensity, frequency shift, and spectral  
844 shape in gaseous N<sub>2</sub>. *J Chem Phys* 59:1706-1712.
- 845 Wang X, Chou IM, Hu W, Burruss RC, Sun Q, Song Y (2011) Raman spectroscopic  
846 measurements of CO<sub>2</sub> density: Experimental calibration with high-pressure optical cell  
847 (HPOC) and fused silica capillary capsule (FSCC) with application to fluid inclusion  
848 observations. *Geochim Cosmochim Acta* 75:4080–4093
- 849 Wells PR (1977) Pyroxene thermometry in simple and complex systems. *Contrib Mineral*  
850 *Petrol* 62:129-139
- 851 Witt-Eickschen G, Seck HA (1991) Solubility of Ca and Al in orthopyroxene from spinel  
852 peridotite: an improved version of an empirical geothermometer. *Contrib Mineral Petrol*  
853 106:431-439
- 854 Wright RB, Wang CH (1973) Density effect on the Fermi resonance in gaseous CO<sub>2</sub> Raman  
855 scattering. *J Chem Phys* 58: 2893–2895
- 856 Wulff-Pedersen E, Neumann ER, Jensen BB (1996) The upper mantle under La Palma,  
857 Canary Islands: formation of Si–K–Na-rich melt and its importance as a metasomatic  
858 agent. *Contrib Mineral Petrol* 125: 113–139
- 859 Zanon V, Frezzotti ML, Peccerillo A (2003). Magmatic feeding system and crustal magma  
860 accumulation beneath Vulcano Island (Italy): Evidence from CO<sub>2</sub> fluid inclusions in quartz  
861 xenoliths. *J Geophys Res* 108:2298 <http://doi.org/10.1029/2002JB002140>
- 862 Zanon V, Frezzotti ML (2013) Magma storage and ascent conditions beneath Pico and Faial  
863 islands (Azores archipelago): A study on fluid inclusions. *Geochem Geophys Geosyst*  
864 14:3494–3514

865 Zaczek K, Troll VR, Cachao M, Ferreira F, Deegan FM, Carracedo JC, Meade FC, Burchardt  
866 S (2015) Nanofossils in 2011 El Hierro eruptive products reinstate plume model for  
867 Canary Islands. Sci Rep 5, 7945. <http://dx.doi.org/10.1038/srep07945>.

868

869

## 870 Figure Captions

871

872

873 Fig. 1 - **a** Geographical setting of the Canary Islands showing the age of the volcanism and the  
874 stages of the volcanic island growth (Shield stage, Post-erosional stage, Post-shield gap),  
875 (modified from Carracedo 1999, Acosta et al. 2005). The yellow lines define the main  
876 structures of Atlantic and African tectonic units; **b** Geographical setting of El Hierro Island  
877 reporting xenolith sampling locality in El Julan cliff Valley (red star).

878 Fig. 2 - **a** ultramafic xenoliths in the basaltic lava outcrop of El Julan cliff Valley; **b – h**  
879 microphotographs of studied peridotites. **b** Deformed olivine porphyroclasts (Ol I) in  
880 spinel harzburgite (XML9, crossed polarizers); **c** Orthopyroxene porphyroclasts (Opx I)  
881 with exsolution lamellae of clinopyroxene (Cpx) in spinel lherzolite (XML8, crossed  
882 polarizers) **d** Exsolved Opx I with rims free of exsolution lamellae in spinel harzburgite  
883 (XML7, parallel polarizers); **e** Opx I without exsolution lamellae in spinel harzburgite  
884 (XML4, parallel polarizers); **f** Olivine neoblasts (Ol II) forming triple junctions in spinel  
885 harzburgite XML7, crossed polarizers; **g** Neoblast assemblage of Ol II + Opx II + Cpx +  
886 Sp in spinel lherzolite (XML3, crossed polarizers); **h** Ol II forming narrow alignments  
887 cutting Ol I in spinel dunite (broken yellow lines) (XML1, crossed polarizers).

888 Fig. 3 - Microphotographs of early Type I fluid inclusions in low temperature (LT)  
889 peridotites; **a** Intragranular trail of Type I fluid inclusions in Ol I (harzburgite XML7,  
890 parallel polarizers); **b** carbonate (high birefringency) in fluid inclusions and microveins  
891 (red arrows) in Ol I (harzburgite XML7, crossed polarizers); **c** cluster of Type I fluid

inclusions in Opx I (harzburgite XML7, parallel polarizers); **d** multiphase Type I fluid inclusion containing several daughter minerals and showing evidence for partial decrepitation (red arrows in Ol I (harzburgite XML7 parallel polarizers)).

Fig. 4 - Raman characterization of daughter mineral phases in a single Type I fluid inclusion.

**a** Photomicrograph showing distribution of daughter mineral phases in inclusion based on Raman mapping: anhydrite (Anh), dolomite (Dol), sulfohalite (Shl),  $\text{MgSO}_4 + \text{H}_2\text{O}$ , apatite (Ap), spinel (Sp), and  $\text{CO}_2 + \text{N}_2$  fluid; **b-f** Raman spectra of daughter mineral phases; **b** apatite; **c** anhydrite; **d** water in  $\text{MgSO}_4 \cdot n\text{H}_2\text{O}$ ; **e** anhydrite, sulfohalite, and dolomite; **f** spinel and anhydrite. Numbers in spectra report Raman modes of identified phases in  $\text{cm}^{-1}$ . Asterisks indicate host mineral vibrations.

Fig. 5 - Microphotographs of Late Type II fluid inclusions in LT and HT peridotites. **a** intragranular trails (red arrows) in orthopyroxene porphyroclast and clinopyroxene; **b** decrepitated fluid inclusions in an olivine porphyroclast; **c** isolated cluster of fluid inclusions (red arrows); **d** fluid inclusions distributed parallel to exsolution lamellae (red arrows) in an orthopyroxene porphyroclast.

Fig. 6 - Histogram of  $\text{CO}_2$  melting temperatures ( $T_m$ ) for Type II fluid inclusions, and final  $\text{CO}_2$  melting temperatures ( $T_m$ ) for Type I fluid inclusions. n = number of measurements.

Fig. 7 - **a** Composition ( $X_{\text{N}_2}$ ) and molar volume ( $\text{cm}^3/\text{mole}$ ) of Type I  $\text{CO}_2 - \text{N}_2$  fluid inclusions from a single cluster. black numbers =  $X_{\text{N}_2}$ ; yellow numbers = molar volume ( $\text{cm}^3/\text{mole}$ ) =; **b** and **c** Raman spectra of  $\text{CO}_2$  and  $\text{N}_2$ ; ( $\Delta$ ) = distance of the Fermi doublet in  $\text{CO}_2$  Raman spectra.

Fig. 8 - Isochore ( $\text{cm}^3/\text{mole}$ ) distribution in the T-X diagram for the  $\text{CO}_2 - \text{N}_2$  system (modified from van den Kerkhof 1988 and Klemm et al. 1992). Measured phase transition sequences for S4 and H3 Type I  $\text{CO}_2 - \text{N}_2$  fluid inclusions of known composition allow

916 determining molar volumes (green dots). S = solid; L = liquid; V = vapor; Th =  
917 homogenization temperature.

918 Fig. 9 - Histogram of CO<sub>2</sub> homogenization temperatures (ThL) for Type II fluid inclusions.  
919 Ol = olivine; Opx = orthopyroxene; Cpx = clinopyroxene; n. = number of measurements.

920 Fig. 10 - Histograms of CO<sub>2</sub> homogenization temperatures (ThL) for Type II fluid inclusions  
921 in LT (a) and HT (b) peridotites. Abbreviations as in Fig. 9.

922 Fig. 11 - Histograms of CO<sub>2</sub> homogenization temperatures (ThL) for Type II fluid inclusions  
923 showing data distribution in the different minerals. Abbreviations as in Fig. 9.

924 Fig. 12 - Distribution of CO<sub>2</sub> density values for Type II fluid inclusions in LT (a) and HT (b)  
925 peridotites. See text, for discussion. Abbreviations as in Fig. 9.

926 Fig. 13 - CO<sub>2</sub> isochore (g/cm<sup>3</sup>) distribution in the P-T diagram for Type I and Type II fluid  
927 inclusions in LT and HT peridotites. Yellow arrows indicate the ascent path of LT and HT  
928 peridotites at the considered temperatures. The pink star indicates pressure conditions  
929 recorded by Type I fluid inclusions in LT peridotites. Green and blue stars indicate  
930 pressures of deep trapping of Type II CO<sub>2</sub> fluids in LT and HT peridotites, respectively.  
931 Red stars indicate pressures of shallow trapping of Type II CO<sub>2</sub> fluids in LT and HT  
932 peridotites, respectively.

933 Fig. 14 - Proposed model for the magma plumbing system of El Hierro volcano at 40-30 ka. A  
934 deep-seated reservoir is identified in the shallow lithospheric mantle at depths from  
935 approximately 37 to 22 km. A short-lived shallower reservoir located in the lower oceanic  
936 crust at 12-10 km. See text for discussion. The black star = source of mantle xenoliths.

Dear Eduardo

First of all, I apologize for it has taken so long to get your manuscript reviewed. This was mainly because one reviewer was away for a long time.

Nevertheless, we now received 3 reviews that are overall positive, and I think that the paper needs moderate to major revision. The reviewers identified several problems and all commented on poor English. For example, one reviewer is concerned that “Manuscript is in need of careful final edits with attention to the small details of grammar, English, and bits of missing text”. As to the manuscript topic, data and conclusions, I agree with Thor Hansteen, who found your results on different daughter phases (“carbonates + sulphates,  $\pm$  chlorides  $\pm$  phosphates  $\pm$  opaque minerals”) are of particular interest, but also considered the implications for the magma ascent from the inclusions’ CO<sub>2</sub> density in your paper to have been reported before and thus being “standard”. This makes me wonder whether you are willing to make your publication more exciting by discussing compositions of the carbonate-sulfate melts in the lithospheric mantle, their origin (big question mark) and contribution to peridotite-derived silicate melts. I personally welcome this new information to be presented in Bulletin of Volcanology, if your submission to Chemical Geology (Villa et al., Halogens in the lithospheric mantle beneath El Hierro) is unsuccessful.

I also agree with Frances Deegan that you make references to other papers without actually discussing other people models in the context of your data. In a covering letter appended to your revised manuscript, you must explain how you have addressed the comments made by all reviewers. If you disagree with any of the comments please clearly explain why.

My recommendations and the reviewers' comments can be found at the end of this email.

**Reviewer #1: Review of the manuscript “Lithospheric magma dynamics beneath El Hierro, Canary Islands:**

a fluid inclusion study” by E. Oglialor<sup>1</sup>, M.L. Frezzotti, S. Ferrando, C. Tiraboschi, C. Principe, G. Groppelli, and I.M. Villa

General comments:

This is a potentially interesting paper with a comprehensive original data set on fluid inclusions in mantle xenoliths from El Hierro Island. The data are utilized to tell an interesting history of mantle fluid origin and xenolith ascent. The new and innovative feature is the detailed description of carbonate and sulphate phases occurring in the early fluid inclusions, indicating a complex chemistry of the originally trapped mantle fluids. However, the fluid inclusion data set is used to describe the magma ascent history of the host magmas and thus make inferences about the magma plumbing system of El Hierro, and the conclusions reached are rather similar to the conclusions forwarded by other authors for other eruptions of El Hierro. Thus the conclusions drawn in the paper are valid and good, but except for the refined suggestions about the nature of early fluid inclusions in the peridotites, they are fairly standard. The manuscript in its present form contains several errors and inaccuracies, and the English should be checked before resubmission. Thus a major (thorough) revision is recommended. The most important points are listed below.

**Response – We have better detailed the rationale of our study in the introduction. Present study reveals the depths of lithospheric sub-Moho magma storage regions at El Hierro. Further, studied rocks are the deepest example of peridotites beneath the Island. In addition, complex metasomatic fluids are reported.**

**Most existing information of the deep internal structure of this volcano are coming from the 2011-2012 eruption’s earthquake hypocenters. Our data collectively allow for the first time to propose a model for**

**the deep magma dynamics beneath the Island. No previous studies on mantle rocks have revealed in a similar detail the deep magma dynamics, although several petrological studies have been performed in mantle xenoliths from El Hierro.**

Selected specific comments:

The Abstract could be more to the point in its opening sentences. Please also indicate that you use xenoliths to reconstruct the stagnation depths in the magma plumbing system of the host lavas. Further, there is no mention of model temperatures used in the barometry calculations for the multi-stage ascent model.

**Response – The abstract has been rewritten following your suggestions**

Methods chapter: There is potential problem with the unusually high pressures you derive from the one early CO<sub>2</sub>-N<sub>2</sub> fluid inclusion with a very high density of 1.191 g/cm<sup>3</sup>. This inclusion is used to address the depth of xenolith origin. Using the equation of state of Holloway (1977), you obtain a pressure of about 1.8 GPa. A density of 1.191 g/cm<sup>3</sup> for pure CO<sub>2</sub> would, however, result in a pressure of 1126 MPa at 950 °C using the EOS of Sterner and Pitzer 1994. Please discuss the validity of such presented high pressures.

**Response – We would respectfully disagree with you here. The relations between P, T, V and X in supercritical fluids of geological interest are expressed by the equations of state. These also consider the attractive and repulsive forces and volumes of molecules (e.g., a and b parameters of van der Waals equation). Thus, equations of state for fluid mixtures should consider the application of mixing rules (i.e., Redlich and Kwong 1949). As a consequence, an equation for a CO<sub>2</sub>-N<sub>2</sub> mixture having the same molar volume of a pure CO<sub>2</sub> fluid will not calculate the same P or T values.**

Discussion chapter: Altogether, pressures are calculated for both early and late fluid inclusions in the xenoliths. Although magma stagnation levels for the host magmas are evaluated from the data, model temperatures shown in the P,T-diagram are set to 1000 °C and 950 °C, respectively. Taken the time the xenoliths were in magma contact, why do you not use estimated magma temperatures? Do the late fluid inclusion trails reach xenolith surfaces? Do some of the late FI coexist with melt inclusions?

**Response - We appreciate this comment. Indeed we needed to be more clear in terms of selection of model temperatures. We added these clarifications in the fluid inclusion sections. We did not use the magma temperatures since the densities of fluid inclusions reflect differences in temperatures of LT and HT peridotites. We have, however, considered as model temperatures the higher values of each interval.**

Abstract

Line 25: “ .. late pure CO<sub>2</sub> fluid inclusions trapped during the ascent into the host magma.” What is the evidence for trapping during ascent? Or do you infer this from the pressure data?

**Response - We infer this from pressure data. Text has been modified.**

Introduction

Line 82-86: You state that the magmas “rest” (stagnate) on their way to the surface, but then write: “Results indicate, for the first time, that the magma ascent in the lithospheric mantle occurs as a continuous migration through a plexus of vertically stacked interconnected magma pockets..”. Please explain.

**Response – We agree that the sentence was contradictory. We have eliminated this part.**

### Geological setting and volcanic history

Line 88-92: Please mention here the various mantle plume hypotheses for the Canary Islands.

**Response – We have added the mantle plume hypothesis and other concurrent hypotheses.**

### Methods

Line 174 -175: Please check the pressure calculations for the mixed CO<sub>2</sub>-N<sub>2</sub> fluid inclusions (see comment above)

**Response – see comment above.**

### Fluid inclusion study

Line 303-309: Do the Late Type II fluid inclusions trails partly extend to xenolith surfaces? Are some trails melt-present (coexistence of melt and fluid inclusions)?

**Response. Trails are not extending to xenoliths surfaces and they do not contain basaltic melt/glass. This is quite commonly seen in deep (mantle depth) fluids trapped in xenoliths. We have better detailed this observation in the petrography of peridotites.**

### Discussion

Line 381: You state: “Fluid inclusions in mantle xenoliths represent either metasomatic fluids in the lithosphere, unrelated to xenoliths transport to the surface, or fluids degassed by the ascending magmas during xenolith ejection at the surface..”

This is unclear: The magmatic fluids may relate to the host magma, or alternatively to an earlier batch of magma at the xenolith source depth. Please reformulate this sentence.

**Response – Reformulated.**

Line 386+: You state: “The densities of metasomatic and magmatic fluids are generally different, since trapping occur at different pressure conditions.” This is inaccurate: There are also large temperature variations at a given depth, according to the presence or absence of magma. Please reconsider this sentence.

**Response - We agree. We have rewritten the sentence “The densities of metasomatic and magmatic fluids are generally different, since trapping occur at different pressure and temperature conditions.”**

Line 405-406: Should read: “...which corresponds to magma stagnation episodes at defined depths..”

**Response - OK**

Line 464: Please delete the sentence “Fluxes of CO<sub>2</sub> probably originated by magma degassing episodes.”

**Response - OK**

Line 497-498: You state. “The densest among Type I CO<sub>2</sub>-N<sub>2</sub> mantle metasomatic fluids suggests 60 km as the minimum equilibration depth in the lithosphere for LT peridotites (grey star in Fig. 14;  $P = 1.80 \pm 0.02$  GPa).” Please reconsider this sentence based on the comments above.

**Response – Data are derived from geothermobarometry of CO<sub>2</sub>-N<sub>2</sub> fluids. We should be aware that deep mantle fluids can be more complex than pure CO<sub>2</sub>. This is evident whenever fluid inclusion studies**



include Raman analyses. Raman in fact represent the most powerful analytical technique to detect small amounts of gaseous species in CO<sub>2</sub>-rich fluids. Most previous studies of fluid inclusions in mantle xenoliths from El Hierro did not detect N<sub>2</sub> in CO<sub>2</sub>-rich fluid inclusions. These studies, however, did not include Raman among the analytical techniques.

Line 541: You state “One main result from present study is that it resolves the geometries of the magma storage system in the lithospheric mantle.” I regret to say that this is strictly not correct. The methods used only indicate pressure conditions based on suggested model temperatures, but give NO evidence of the remaining magma plumbing geometry. Please reformulate this sentence.

**Response - We agree. We have deleted all text parts dealing with “geometry” of the magma storage system.**

Conclusions

Line 561-562: You state: “Our observations are consistent with a deep magma source beneath El Hierro volcano, in agreement with the previous models for last eruption in 2011-2012”. This is not to the point as your paper is about magma plumbing systems and ascent, not about magma sources.

**Response - We agree. We have eliminated the sentence.**

Line 563-565: You state: “Finally, present paper demonstrates the potentiality to study the geometries of deep magma reservoirs by fluid inclusion studies in peridotites, when combined with detailed petrological investigations of rocks”. This is too general and thus unfocussed. Please reformulate.

**Response - We agree. We have eliminated the sentence.**

Technical comments:

Please do not start mineral names with a capital letter (as in the captions to Figures 4 and 5)

**Response. We have fixed it.**

Best wishes

Thor Hansteen

**Reviewer #2: Review of “Lithospheric mantle dynamics beneath El Hierro, Canary Islands: a fluid inclusion study” by Eduardo Ogliarolo et al., submitted to Bulletin of Volcanology.**

The manuscript by Ogliarolo et al. presents new fluid inclusion data on ultramafic xenoliths from El Hierro, Canary Islands, in order to contribute to a clearer picture of the magma plumbing system beneath the island. The authors' new results show that El Hierro magmas originate from vertically stacked reservoirs in the lithospheric mantle, which is consistent with the results of previous thermobarometry studies (e.g. Stroncik et al., 2009; Longpre et al., 2014). Overall, I think that this work will make a worthy contribution to our understanding of magma storage and ascent at ocean island volcanoes. However, I have some issues with how the paper is written and I think that it needs an overhaul of the writing in order to improve grammar and syntax and hence accessibility (the figures are of good quality). An improved writing style will require a little more effort but will help the results to be assimilated more easily by the community. I also think that the literature needs to be integrated into the discussion more fully. At the moment, many papers

are cited but not really discussed and compared to the new data. Finally, I think that the authors can make more of an effort with the thermobarometry aspect in terms of updating their own calculations, comparing them to the literature data, and linking them with their new fluid inclusion data. I feel that this would help to strengthen the paper's conclusions.

Some points are expanded on below:

1. The existing literature should be better integrated and discussed in this paper. For example, the introduction and geological background of the manuscript lack a balanced overview of the recent literature on the geology of El Hierro and, in particular, the 2011-2012 submarine eruption. You have mentioned some of the efforts that have been employed to characterize magma dynamics at El Hierro (lines 61 – 64), but you have overlooked a body of work concerning the “floating stones” that were erupted in 2011-2012 and their implications for magma dynamics and magma plumbing at El Hierro (e.g. Troll et al., 2012 in *Solid Earth*; Zaczek et al., 2015 in *Scientific Reports*; Berg et al., 2016 in *Bulletin of Volcanology*). Where you mention “independent analytical approaches” that have been employed to study the plumbing system at El Hierro on line 65, you should also mention “xenolith studies” and cite some relevant literature. The floating stones were highly informative regarding our understanding of magma transport and crustal interaction at El Hierro. I realise that the shallow plumbing system is not the focus of your study, but this work should be at least mentioned in your introduction in order to put your study into context. Furthermore, a review of the 2011-2012 submarine eruption was published in *Earth Science Reviews* in 2015 by Carracedo et al. (<http://dx.doi.org/10.1016/j.earscirev.2015.06.007>). This paper offers a detailed review of the events leading up to, and during, the 2011-2012 eruption and includes discussion of the plumbing system at El Hierro making it highly relevant to your study. Lastly, Longpre et al. have recently published volatile data obtained on samples from the 2011-2012 in *Earth and Planetary Science Letters*, which may be very useful for discussion of your data (Longpre et al., 2017).

**Response - We agree. We were missing some relevant literature. In the present version of the manuscript we have added and discussed all literature indicated by you, including Carracedo et al., 2015, Longprè et al., 2017, Zaczek et al., 2015. In particular, data from Longprè suggesting very deep degassing of CO<sub>2</sub> El Hierro mafic magmas well agree with our finding of CO<sub>2</sub> fluids at pressure of 1 GPa.**

2. I think it would be worthwhile to look into the literature regarding other Canary Islands too. For example, Barker et al. 2015 (DOI 10.1007/s00410-015-1207-7) use mineral thermobarometry and mineral-melt thermobarometry to define the sub-volcanic magma plumbing system for La Palma, Canary Islands. These authors found evidence for magma storage at sub-Moho depths of up to 50km and they discuss various magmatic processes during magma storage such as recycling of pre-existing ocean island plutonic complexes. This paper is thus highly relevant to your work on the deep plumbing system at El Hierro and ought to be discussed.

**Response - We are grateful for this comment. We have discussed data from La Palma by Barker and coauthors, which, as you suggested, share several similarities with present results.**

3. Many of the literature citations in the text do not match the reference list or cannot be found there. These occurrences are too numerous to list here. Please check all literature citations very carefully. Also avoid a) and b) where not necessary e.g. Frezzotti and Peccerillo (2004) does not need to be written as Frezzotti and Peccerillo (2004a).

**Response - We have corrected these issues.**

4. Regarding thermobarometry, have you tried using your pyroxene data to calculate crystallization temperature and pressure? I suggest using several models and also incorporating more recent approaches (it seems to me that you have used fairly old models) and comparing the outcomes. Do you get consistent values? Are these values consistent with the results of your fluid inclusion study? Please see Geiger et al. 2016 in Scientific Reports (DOI 10.1038/srep33629) and references therein for some examples of recent model developments in thermobarometry, with particular application to alkali systems. It would make your paper a much more useful contribution stronger if you follow up on the thermobarometry more thoroughly and link it to your fluid inclusion data. If it turns out that other thermobarometric models are not suitable for your samples, then explain why.

**Response – We respectfully disagree. We have not used fairly old geothermobarometers. We have applied geothermobarometry based on mineral equilibria in mantle rocks. Melt-mineral geothermobarometry in host basaltic rocks is not part of present study.**

5. The manuscript text needs substantial polishing before it is publication-ready and I suggest that you ask a colleague to carefully proof-read your manuscript text for fluency before resubmission. I also think that you need to make very clear the reasons for undertaking this study. As noted above, the plumbing system beneath El Hierro has been extensively studied already. What new insights can your method of choice bring?

**Response – We agree. We have carefully rewritten the text. The new insights of our methods are on the deep internal structure of the volcano. When rewriting the text, we have clarified this issue.**

If the authors can address the points above then I think that this paper would make a welcome contribution to our understanding of the plumbing system at El Hierro, but it first needs to undergo major revision. I would be happy to re-read a revised version.

With best regards,

Frances Deegan, Uppsala University, April 2017

### **Reviewer #3: Hello**

I think this paper is pretty good. It really needs a careful final edit, however, looking for mistakes of grammar and English, as well as putting in a few missing words here and there.

Below are specific issues I found that I think need to be changed or thought about, and most involved making the paper read more clearly, and limiting overly dramatic and overreaching language that is not needed in this paper. Below are some specific examples of edits to consider, but they are not all the small issues. Please comb over carefully.

Cheers.

Abstract

18-19

This opening sentence needs rewriting. Fluid inclusion studies are one example of petrologic investigations, not a unique field themselves, and volcanological data (as I think of it) do not actually help define or constrain any of the parameters of depth of storage, or pathways through plumbing. Petrology does.

**Response - We agree. We have changed the text following your suggestions.**

31-34

Here again...the term (or phrase) 'eruption dynamics' is not appropriate here. This is not what this study is showing. There is nothing about 'eruption dynamics' at all in these data. It would more appropriate to refer to "magma dynamics".

**Response - We agree. We have changed the text following your suggestions.**

These FI data are providing data to infer what conditions the magma (or more correctly, the xenoliths) had experienced. The data are from a 'time' that is well before the 'eruption' and may not have any bearing on the eruption dynamics at all. This is important. The study is about magma pathways and storage levels during ascent from the mantle and through the crust, not about the dynamics of an eruption.

**Response - We agree. We have changed the text following your suggestions. Present study further allows presenting a model for magma pathways that is very similar to magma dynamics during the 2011-2012 eruption. In additions, xenoliths are hosted in erupted lavas.**

34-37

Here it is finally right. This is about magma dynamics, and whether magma dynamics inferred from 50ka FIs show the same/similar behavior as the recent erupted magma.

**Response – We agree. See comment above.**

Introduction

39-40

Cut 'prerequisite'...redundant with essential..."Modelling...is essential to evaluate the monitoring strategies..."

**Response - We agree. We have changed the text following your suggestions.**

41

Cut hence..."pressure and depth"...

"Rest"...better to say "storage and/or accumulation".

**Response - We agree. We have changed the text following your suggestions.**

55-58

Do you mean these studies have already been carried out? Sounds like they have not been... 'Proposed' probably meant to say 'performed'.

**Response - We agree. We have changed the text following your suggestions.**

64

The proposed model...

76

(2004), we have performed...

80

...magma ascent and periodic storage...

81

Cut out "...for the first time..." . May or may not be true and hard to verify.

81-84

**Response - We agree. We have changed the text following your suggestions for all points listed above.**

This last sentence of the intro seems to contradict the earlier setup, and perhaps the data to follow. Either the magma pauses or is stored long enough for fluid to invade and be trapped by host crystals, or not. To say that magma ascent is a "continuous" migration is likely an overreach at this point since discreet levels have been identified using geophys and are likely regions of pooling, or storage areas...direct contradiction to the idea that magma is in a continuous migration!

**Response - We agree. We have changed the text following your suggestions.**

Geo Setting

Generally OK.

Methods

Fairly clearly written.

Comp and P-T...

192-201

Rewrite this paragraph to be more succinct. Is the flow the same as Carracedo's 2001 lava, or different? There should be no confusion, and no need to deduce if it is the same. Did you walk from Carracedo's site to yours and know it's the same? It is or it isn't. It probably doesn't really matter, and this paragraph is overcomplicating the issue. So, it's about 50ka or a bit younger based on Carracedo's ages in the area on similar flows.

**Response - We have simplified the text following your suggestions.**

203-204

"The contours of rocks are sharp"...what does this mean, angular? Clean? Do they have any basaltic coating? You say they have limited host lava infiltrations? Please clarify with a picture or better description. Since you have seen some infiltration, this implies the xenos are warm to hot. How might this affect the preservation of the FI, and their chemistries? Do the xenos show any melt channels forming?

**Response - Angular. Xenoliths with evidence for lava infiltrations were not selected for mineral geothermobarometry and fluid inclusion studies. We have changed the text.**

## Petrography

Written OK, but I have to say that after reading the petrologic description, I have questions about faithful, robust records preserved. The description suggests significant recrystallization and perhaps areas of remelting. Hmmm. Is this a problem?

**Response - Xenoliths show protogranular textures with minor of solid state recrystallization (< of 30 %). This is indicative of moderate recrystallization at mantle depths. In higher temperature xenoliths (900°C), evidence for variable sub-solidus heating is revealed by the presence of neoblasts and non clear opx porphyroclasts. Microstructural evidence for incipient melting of xenoliths in ascending lavas is absent in studied peridotites. Cpx and or spinel do not show evidence of incipient melting (e.g., spongy rims).**

## Mineral Chemistry

Noting that Ca increases in some neoblastic Ol is important. What is this saying about CPX? Is there a history of heating these xenos and melting of CPX? Does it matter, or not?

**Response – Evidence for melting of Cpx is absent (i.e no spongy texture). In addition, Cpx is in textural equilibrium with the other mineral phases. Local heating is observed to about 1100°C degrees limited to Opx neoblasts. The Ca content of Cpx is considered by the two-pyroxene thermometer, and by the solubility of Ca and Al in orthopyroxene in equilibrium with olivine, clinopyroxene and spinel thermometer.**

## Geothermobarometry

I am concerned about these equilibrium temperature estimates...ALL seems too cool to be correct for these rock compositions. Shouldn't these temps be more >1100-1200C if they formed in the mantle? I suspect these are re-equilibration temperatures from being in the basalt. This is not clearly stated here (I see it later.), and the reader should be assured the authors know that the minerals used for FI have been survived r-e without leaking or cracking FI.

**Response – We respectfully disagree. Calculated temperatures for peridotites are not too cool at the considered depths in the mantle. They correspond to geotherms with heat flow > 70 mW/m<sup>2</sup> at 60 - 65 km depth. We imagine that “too cool” is referred an oceanic mantle geotherm.**

## Fluid Inclusion Study

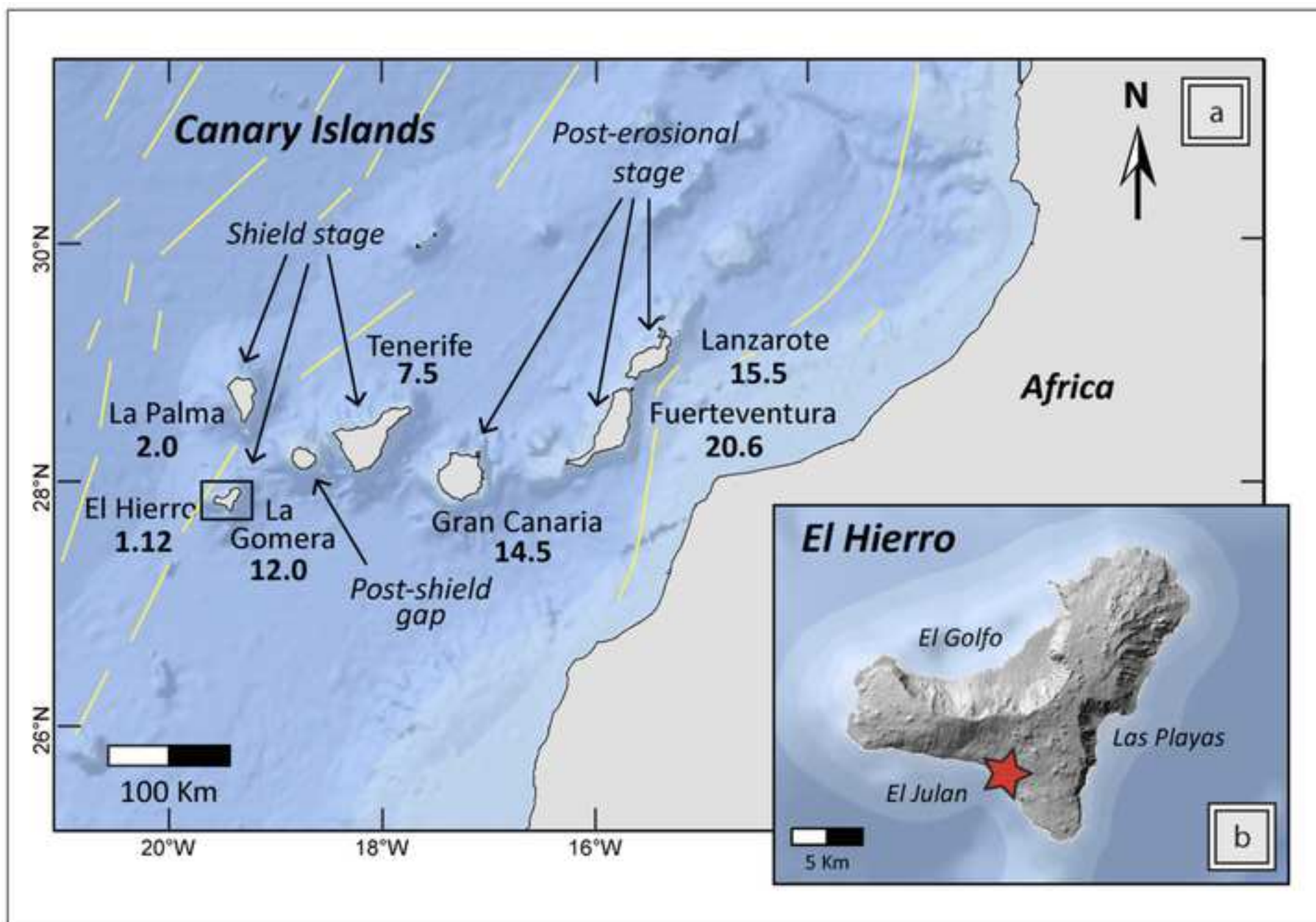
This most important section is well-written and descriptive.

## Discussion and conclusion

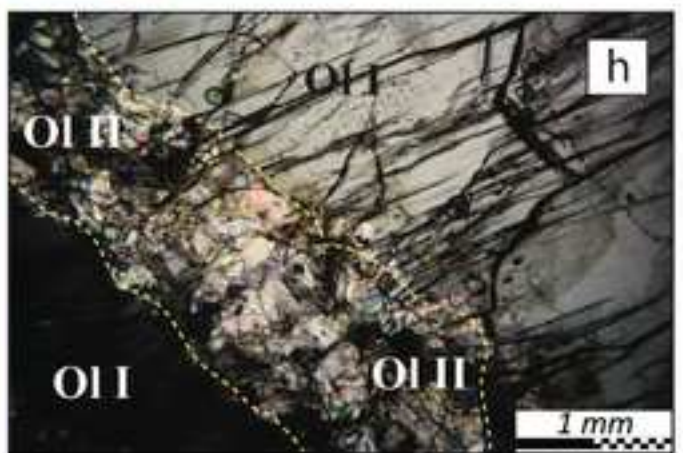
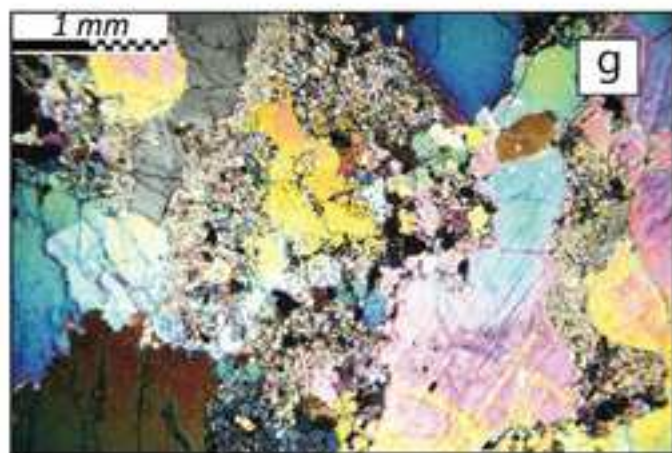
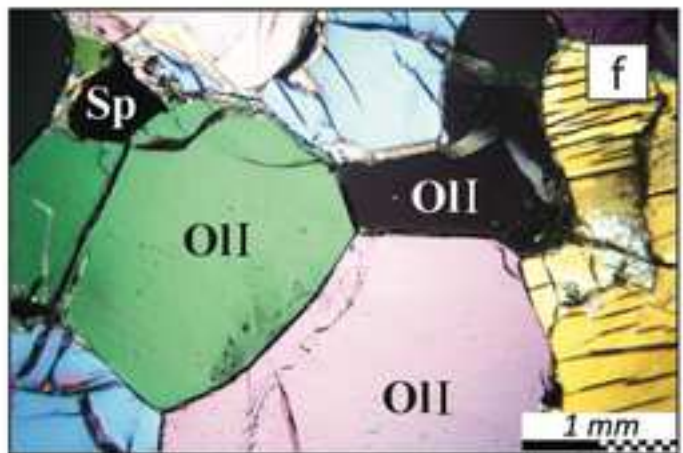
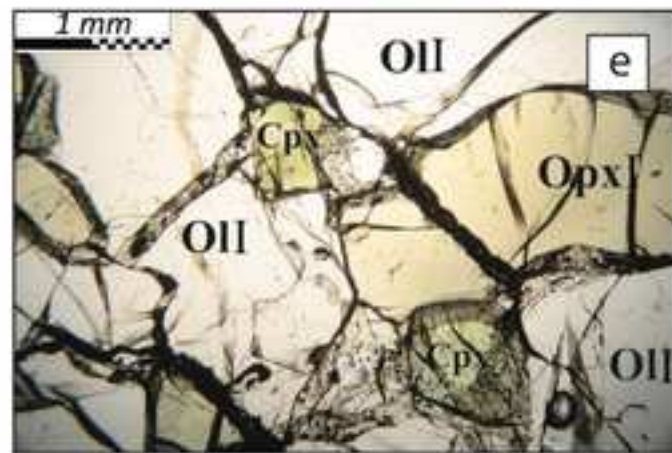
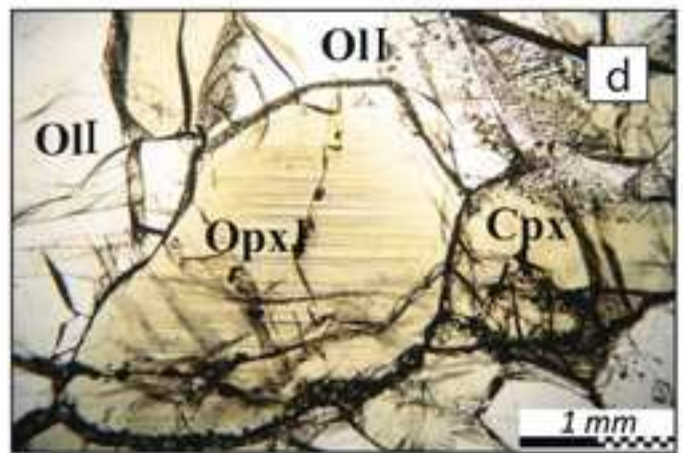
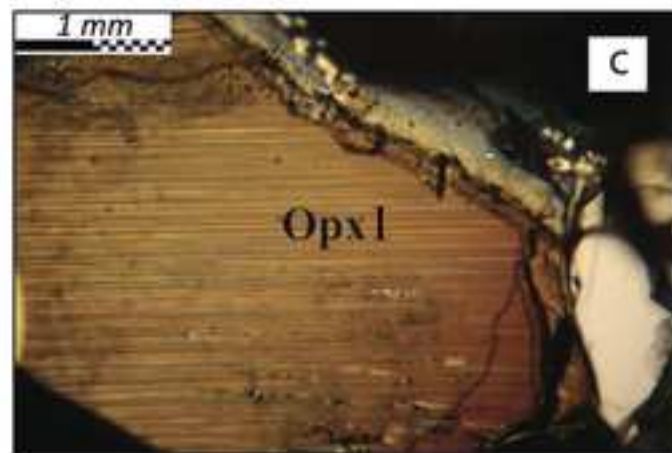
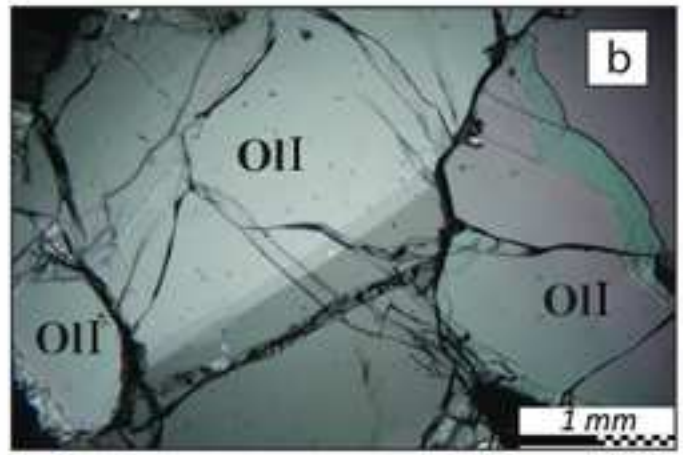
I liked these sections. Well written and described. My only criticism is the over statement that this study somehow reveals "geometry" of the magma plumbing system. It really does not. These data only tell that some components of the magma were sourced deep, then stored at mid and shallow crustal levels. Beyond the presumption that there is a vertical movement of material beneath El Hierro (as generally believed for any volcano), no other geometric info can be gleaned. Dial back these statements to be more considerate of this fact. FI data verify what the geophys already sees.

**Response – We agree with you. We have eliminated the word: geometry.**

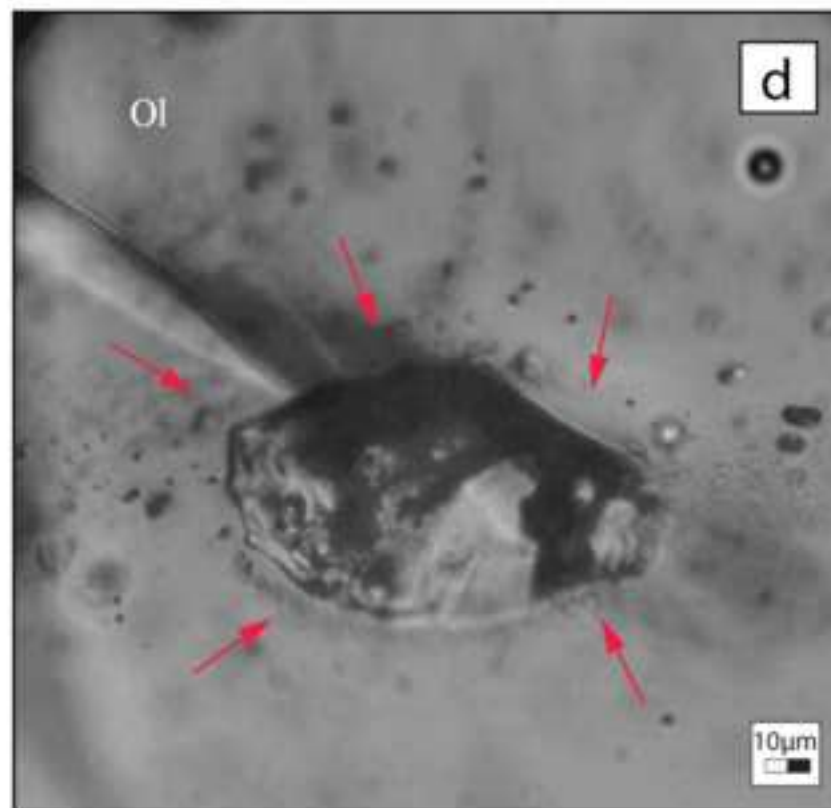
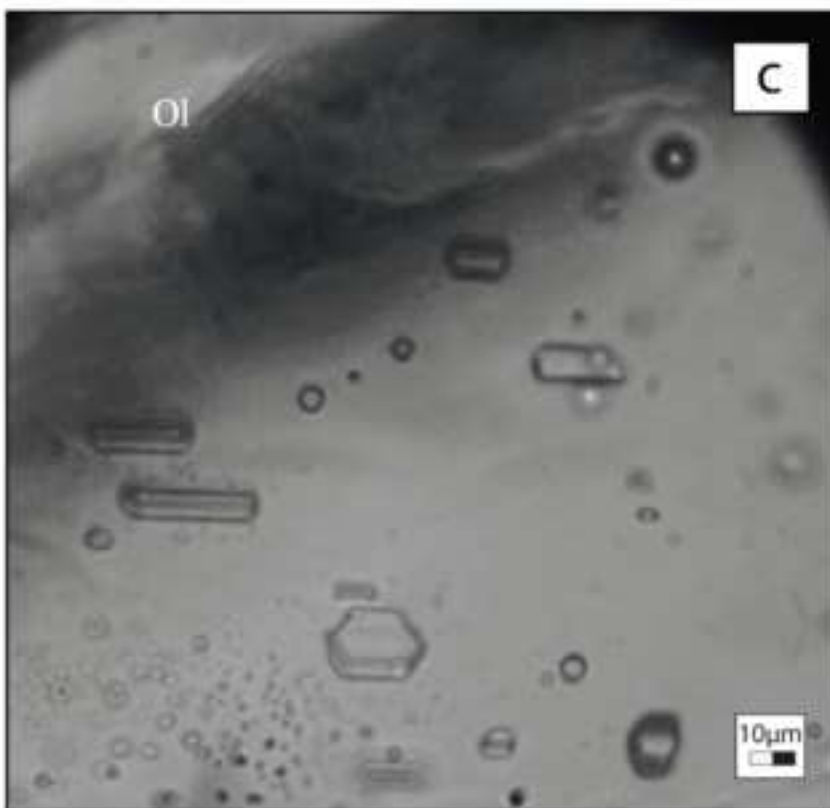
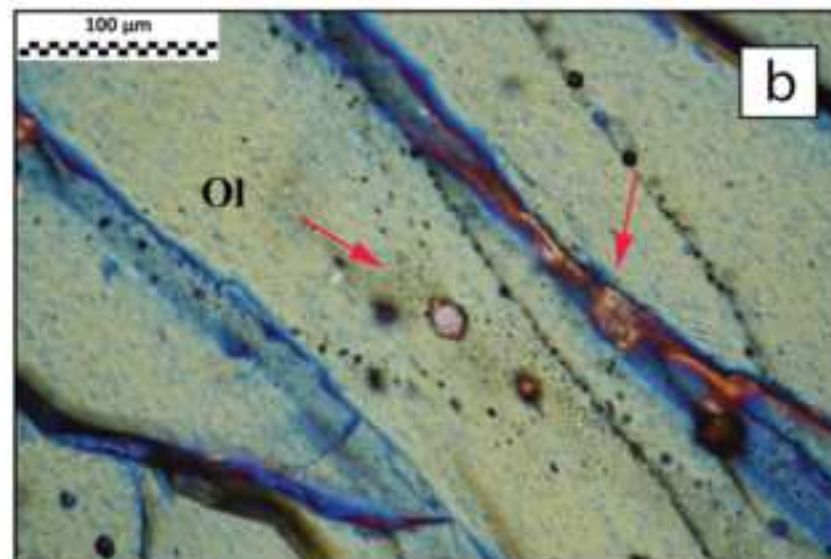
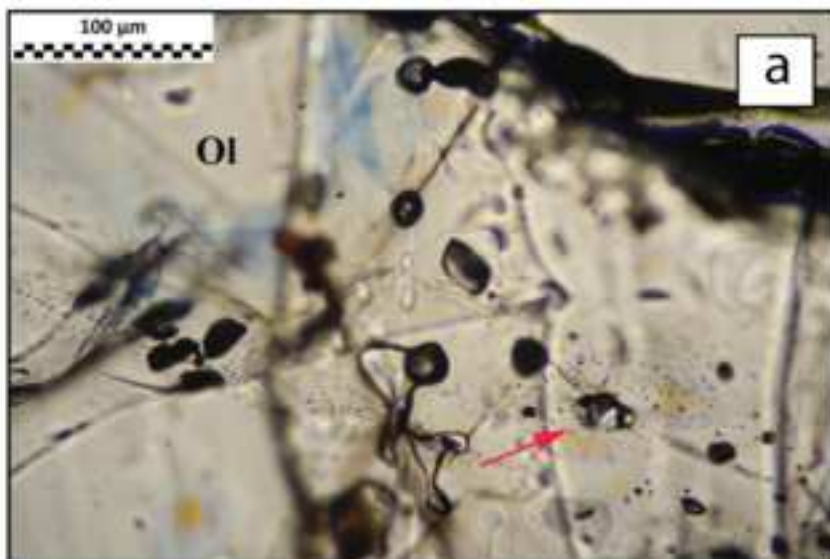
Good overall.

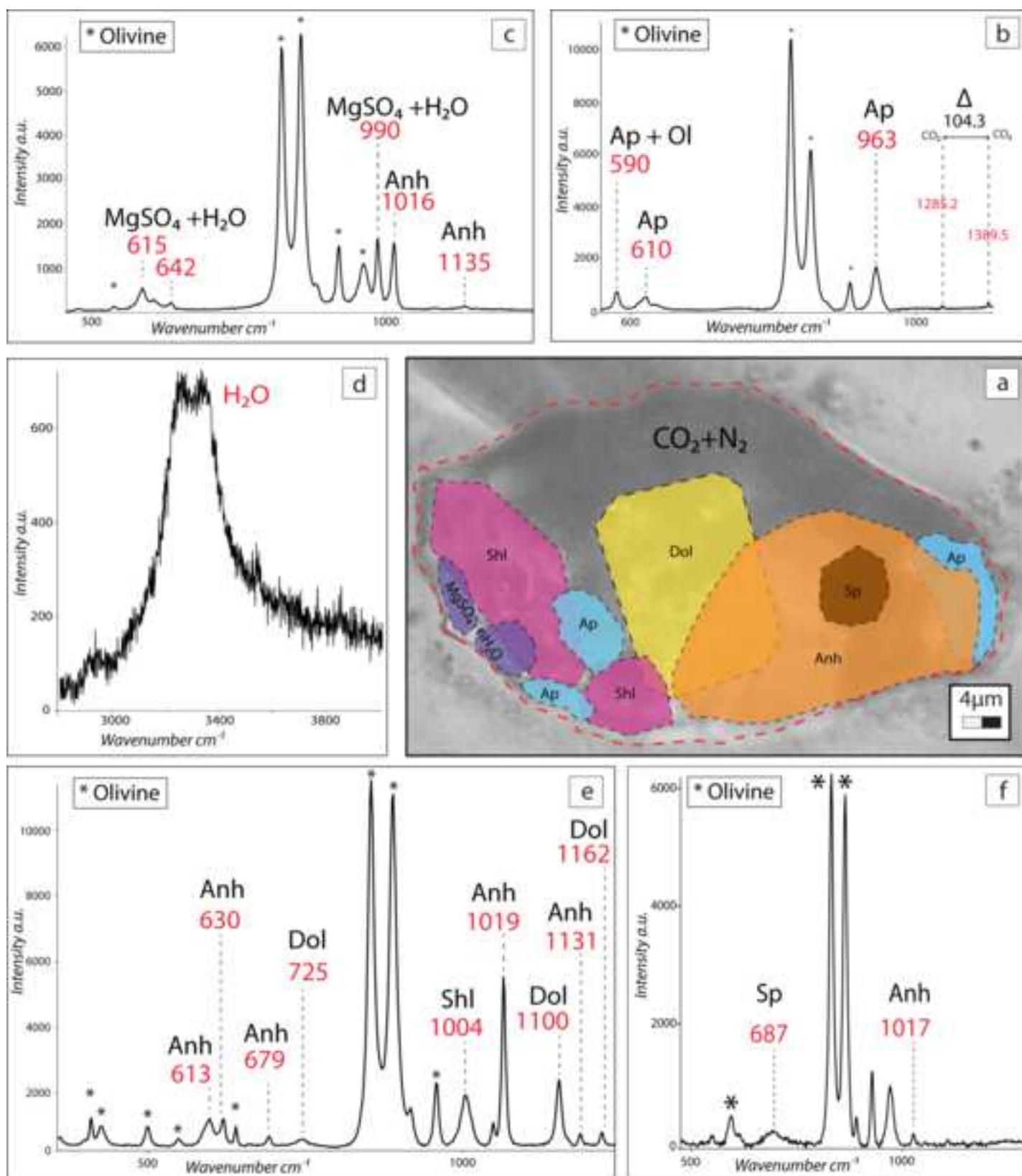




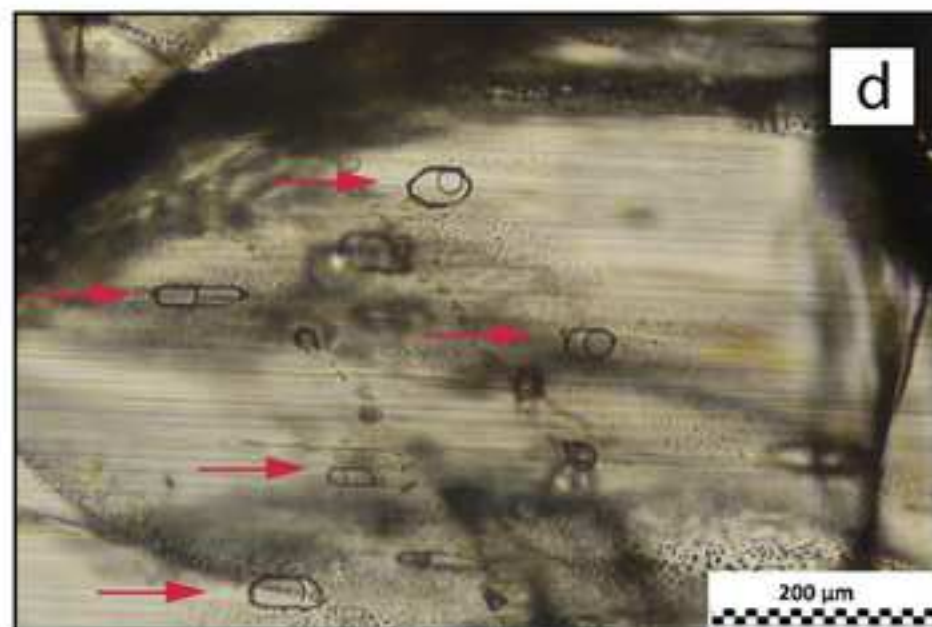
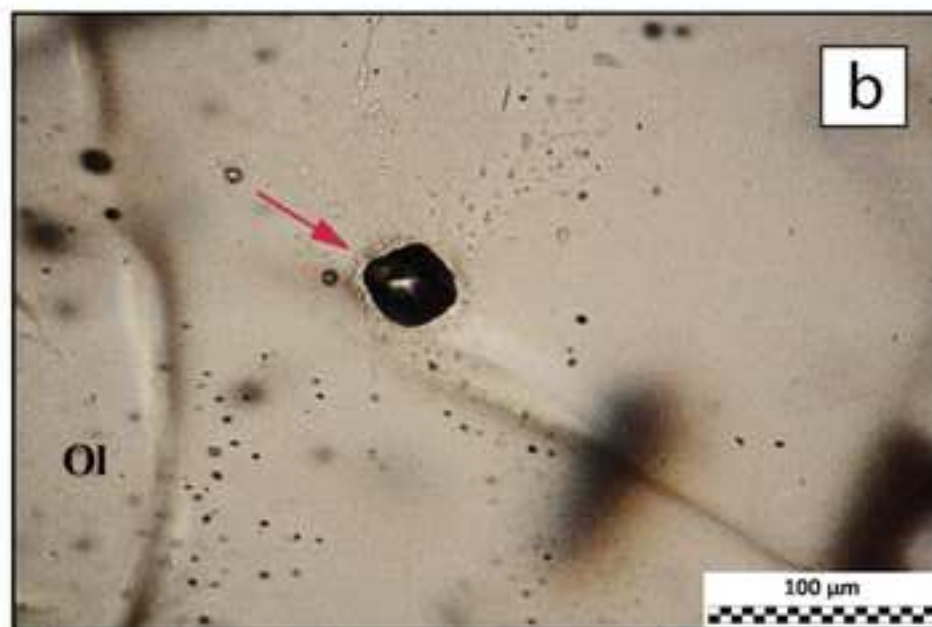
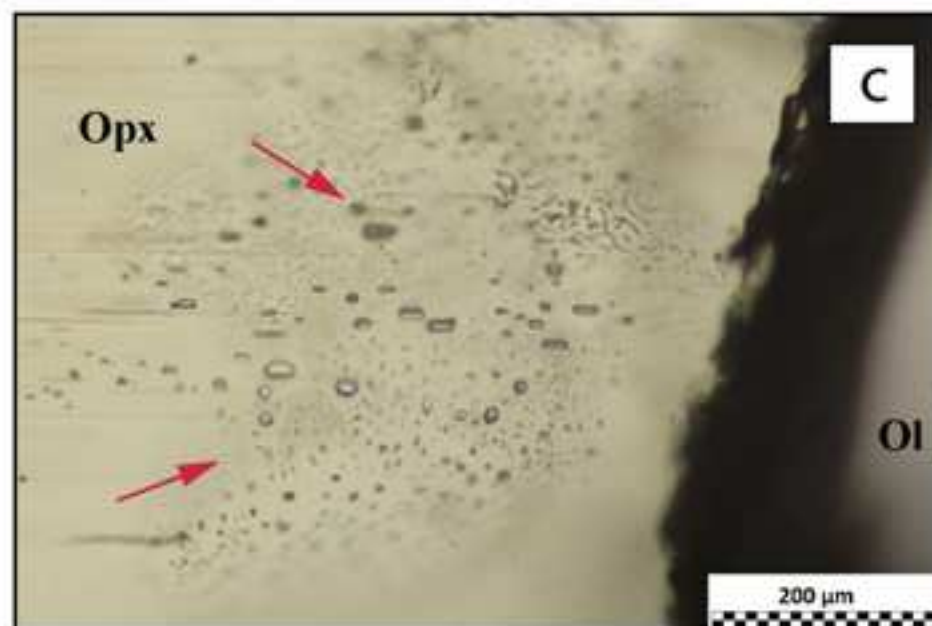
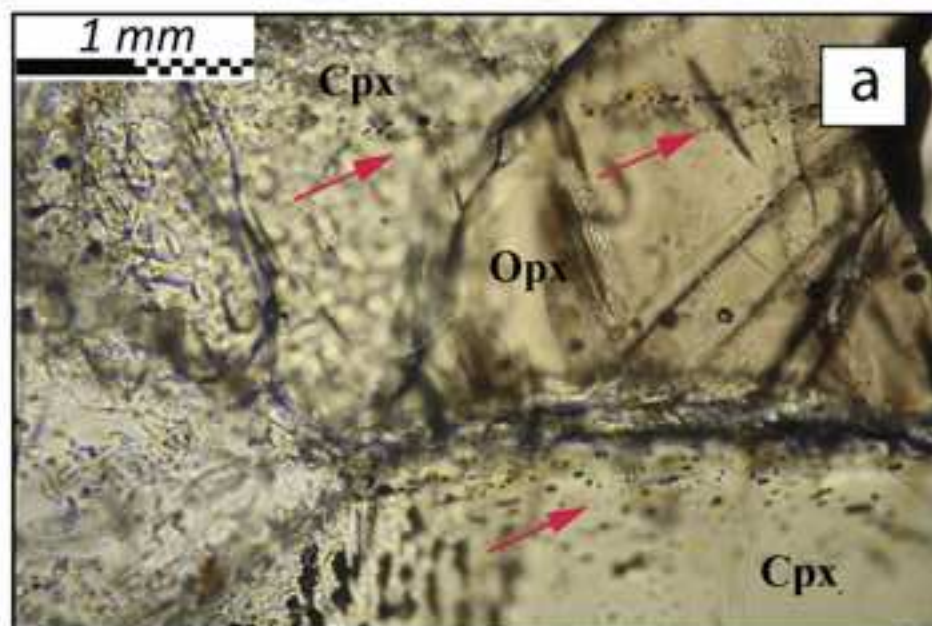












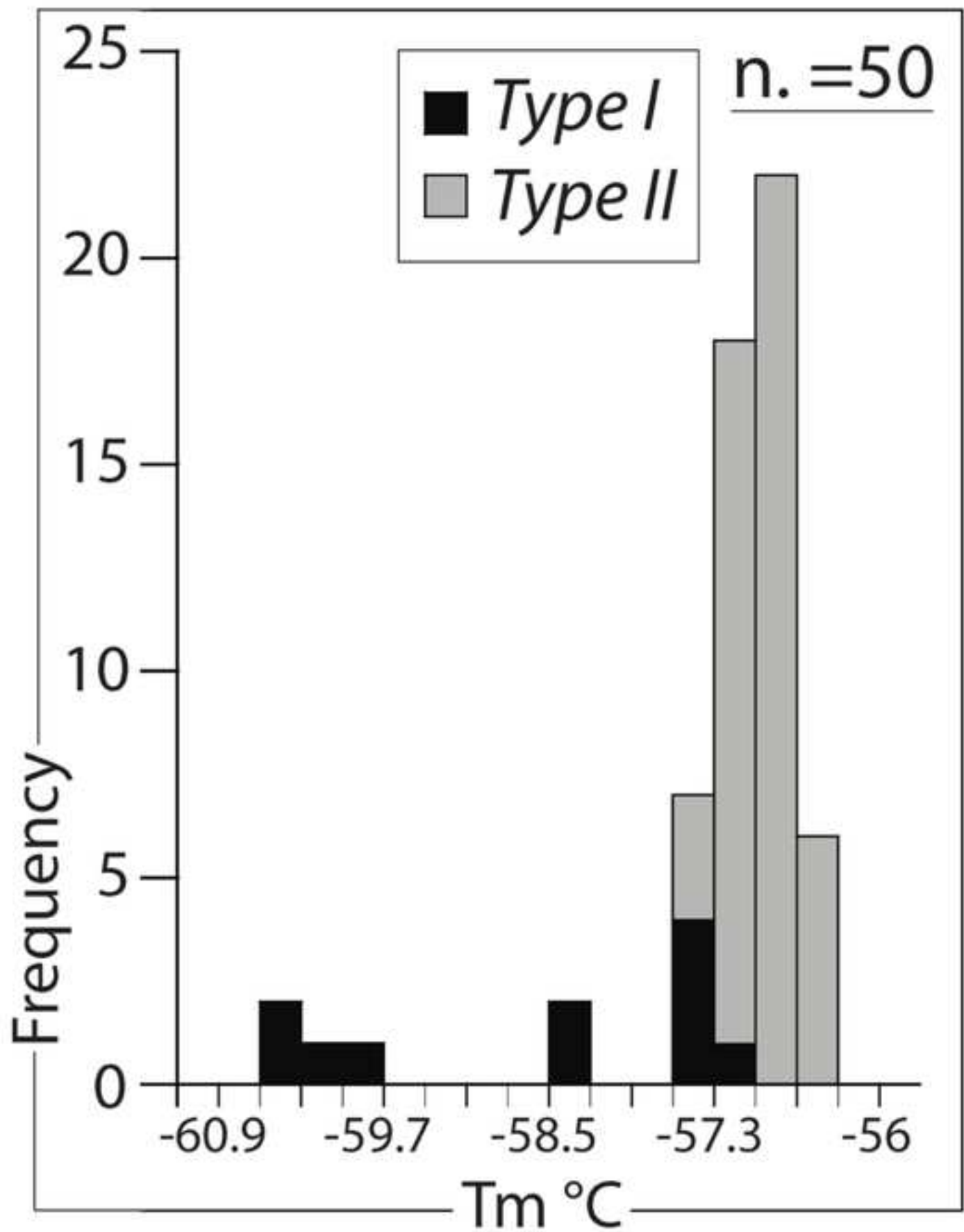


Fig. 7 PDF

